applied sciences

IMPACT FACTOR 2.5

CITESCORE 5.3

Article

CMM Influence Factors and Uncertainty Associated with Length Measurement

Alistair Forbes

Special Issue
Advanced Studies in Coordinate Measuring Technique

Edited by
Prof. Dr. Adam Gąska

MDPI

https://doi.org/10.3390/app15010271

applied sciences

MDPI

Article

CMM Influence Factors and Uncertainty Associated with Length Measurement

Alistair Forbes

National Physical Laboratory, London TW11 0LW, UK; alistair.forbes@npl.co.uk

Abstract: This paper is concerned with coordinate measuring machine (CMM) uncertainty evaluation, in particular, the uncertainties associated with point clouds and distances derived from the point cloud. The uncertainty evaluation approach is model-based following the principles of the Guide to the Expression of Uncertainty in Measurement and the law of the propagation of uncertainty. The paper considers a range of CMM influence factors and derives an explicit dependence for the point cloud data coordinates on the influence factors, allowing uncertainties associated with the influence factors to be propagated through to point cloud uncertainties. The paper describes the use of Gaussian processes to model kinematic and probing errors using a small number of statistical hyper-parameters. These models permit an explicit statement of the uncertainty associated with point clouds and length measurement, enabling the latter to be compared directly with a statement of the maximum permissible error in length measurement. The uncertainty evaluation methodology is direct in that it requires no optimisation nor Monte Carlo simulations.

Keywords: coordinate metrology; Gaussian process models; length measurement capability; uncertainty evaluation

Academic Editor: Adam Gąska

Received: 28 November 2024
Revised: 19 December 2024
Accepted: 24 December 2024
Published: 30 December 2024

Citation: Forbes, A. CMM Influence Factors and Uncertainty Associated with Length Measurement. *Appl. Sci.* **2025**, *15*, 271. https://doi.org/10.3390/app15010271

1. Introduction

The primary task of form and tolerance assessment in precision engineering is to estimate how close a manufactured workpiece is to its ideal geometry, as specified by a technical drawing or CAD specification. Traditionally, such assessment was made using hard gauges, but in recent decades, coordinate measuring systems [1] such as coordinate measuring machines (CMMs) are used extensively in industry for this task. In order for CMMs to perform this task in a way that supports trustworthiness and interoperability, it is necessary to establish the traceability of CMM measurement to the metre [2]. As part of establishing metrological traceability of any measurement system, it is necessary to evaluate the uncertainties associated with the measurements made [3]. However, the evaluation of the uncertainty associated with CMM measurement is not straightforward [4]. CMM measurements are subject to a large range of influence factors including kinematic errors, probing effects and environmental effects that are difficult to quantify and considerable effort has to be made in order to provide valid uncertainty estimates associated with a particular measuring task.

There are two general approaches to evaluating uncertainties associated with a measurement system. The first, often termed measurement systems analysis (MSA), is to perform a number of experiments in which the influence factors (tool, operator, environment) are deliberately varied and the variation in the measured results is assessed using analysis of variance techniques (ANOVA) to quantify the contribution of each influence factor to the observed variation [5–8]. This approach is sometimes referred to as an *a posteriori*

approach in that the uncertainty evaluation can only be performed after the experimental results. The second approach, as described by the Guide to the Expression of Uncertainty in Measurement (GUM, [3,9,10], is model-based and relies on an input–output model that describes the measurement result as a known function of the influence factors. Assigning means and variances (and distributions) to the influence factors allows, in principle, means and variances (and distributions) associated with the measurand to be estimated.

The two approaches to uncertainty evaluation associated with coordinate metrology were addressed by a recent European project *Evaluation of uncertainty associated with coordinate metrology*—EUCoM; [11]. The first, observation-based approach is based on taking multiple measurements of the same artefact in a number of positions within the working volume of the CMM, specifically, five repeat measurements in each of four positions. This approach is designed to assess the repeatability component of uncertainty, along with the effect of the geometric errors of the CMM that vary with location within the working volume. An analysis of variance approach is used to assess the uncertainty contributions from repeatability and the geometric errors [12,13].

This paper is concerned with a model-based approach to evaluating CMM uncertainty. The virtual CMM (VCMM) concept, see, e.g., [14–19], is an established example of a model-based approach for CMM uncertainty evaluation. The VCMM approach involves (i) a comprehensive model of the CMM behaviour, including the kinematic errors, involving the order of 100 or more model parameters, (ii) a detailed statistical characterisation of the model parameters, and (iii) a Monte Carlo approach [9,10] for propagating the uncertainties associated with the model parameters through to the features derived from the point cloud data. While the VCMM approach potentially is the method of choice for CMM uncertainty evaluation, it does suffer from a number of drawbacks: (a) it requires a large number of parameters to be characterised statistically, often through extensive measurement exercises involving multiple measurements of artefacts such as ball plates [20–22], (b) the statistical characterisation of the parameters may not reflect the behaviour of the CMM at later times or in different environments, and (c) there is considerable computation required to implement this in software.

The approach described in this paper and developed during the EUCoM project follows a model-based approach, as used in the VCMM methodology, but with two simplifications. The first exploits the fact that the dependence of the measured point coordinates $\boldsymbol{x}_i$ on the influence factors can be modelled explicitly, which enables the sensitivity with respect to the influence factors to be determined analytically (to the first order). The sensitivity of derived features such as distances and differences in distances can also be determined analytically. The second simplification is to employ approximate models of CMM kinematic errors and probing effects based on Gaussian process models [23]. The models are approximate in the sense that in the absence of information about the actual kinematic or probing errors, the models describe plausible behaviour of the CMM. We also note that these models apply to CMMs that are assumed to be error-corrected already so that the models are required to describe the departure of the CMM's actual behaviour from its modelled behaviour rather than account for the kinematic and probing errors themselves. The models are being used to estimate the uncertainty contributions from the various influence factors, not to evaluate or estimate (and correct for) the influence factors themselves. This means that some of the complexity of error correction can be avoided. This second simplification enables, firstly, the approximate models to be specified by a small number of statistical parameters and, secondly, the sensitivity of the points coordinates with respect to the modelled kinematic and probing errors to be calculated using simple formulæ involving the statistical parameters. Using the approximate models, the uncertainty behaviour of a CMM for a range of influence factors considered in this paper can be specified in terms of

the 12 statistical parameters listed in Table 1 and defined in Sections 4 and 5. The methods described in this paper represent an attempt to achieve a functionality as close as possible to that of a VCMM capability but using models that are as simple as possible but no simpler.

The GUM differentiates between two methodologies, Type A and Type B, for associating uncertainties with effects. A Type A approach, usually applied to repeated measurements, involves a statistical analysis of the data in order to assign an uncertainty, e.g., derived from the standard deviation of repeated measurements. A Type A approach can be regarded as an *a posteriori* approach. According to the GUM, a Type B approach involves assigning uncertainties to influence factors using other information, such as previous measurements, manufacturer's specifications, experience or expert judgement. As such, a Type B evaluation can be thought of as an *a priori* approach, as these assignments can be made before measurements are made.

The approach described in this paper largely follows a Type B approach and addresses uncertainty evaluation on the basis of information that is available a priori. This prior information is encoded in the values of statistical hyper-parameters associated with the various influence factors considered. These parameters can be thought of as specifying a population of CMMs that are consistent with the parameter values, e.g., CMMs that have squareness errors in a plausible range, etc. If we draw a number of CMMs from this population and use them to perform a particular measurement task, such as measure the length of a gauge block, we will obtain a range of measurement results. The uncertainty evaluation methodology described attempts to provide a statistical characterisation, in terms of uncertainties, of what that range would be if we were able to perform these experiments. Many of the influence factors, such as a squareness error associated with CMM measurements, can be thought of as systematic in that they persist and stay approximately constant in the time taken to perform a measurement task. The GUM Type B methodology enables the uncertainty contribution associated with these systematic effects to be evaluated.

The remainder of this paper is organised as follows. The application of the GUM methodology to point cloud data is discussed in Section 2. Although this paper is mainly concerned with CMM length measuring capability, Section 3 discusses CMM length measuring capability in the context of three-dimensional measurement capability, showing that the length measuring capability can only partially characterise CMM performance. Point cloud uncertainty evaluation for repeatability effects, probe qualification effects and scale and squareness effects are discussed in Section 4. Section 5 discusses Gaussian process models to represent kinematic errors, such as straightness, roll, pitch and yaw, and probing errors and how these models can be used to evaluate point cloud uncertainties. Section 6 describes how the uncertainties associated with the influence factors propagate through to uncertainties associated with length measurement. The section also discusses how a statement of length measuring capability such as maximum permissible error can be used to guide the assignment of the statistical parameters for the influence factors. Section 7 illustrates the uncertainty evaluation methodologies related to the measurement of a step gauge artefact. Our concluding remarks are given in Section 8.

Notation

Given coordinate data $\boldsymbol{x}_i$, $i = 1, 2, \ldots m$, then $\boldsymbol{x}_{1:m} = (x_1, y_1, z_1, x_2, \ldots, z_m)^\top$, i.e., $\boldsymbol{x}_{1:m}$ represents the $3m \times 1$ vector of coordinates in the given order. Table 1 gives a summary of the notation used in this paper relating to CMM influence factors and associated statistical parameters, while Table 2 gives a summary of the notation relating to variance matrices.

Table 1. Notation and statistical hyper-parameters associated with CMM influence factors; see Sections 4 and 5.

Symbol	Association, Interpretation
MPE	Statement of maximum permissible error
A, B	Parameters characterising the MPE as a function of distance, $A + d/B$
R	Repeatability
σ_R	Standard deviation associated with repeatability
PQ	Probe qualification/location effects
σ_{PQ}	Standard deviation associated with probe qualification effects
S	Scale and squareness effects
σ_S	Standard deviation associated with a global scale effect
$\sigma_{S,a}$	Standard deviation associated with independent scale effects associated with each axis
σ_Q	Standard deviation associated with independent squareness effects
ET	Geometric location errors (local scale and straightness)
σ_{ET}	Standard deviation associated with spatially correlated geometric location errors
λ_{ET}	Length scale parameter associated with the spatially correlated geometric location errors
ER	Geometric rotation errors (roll, pitch and yaw)
σ_{ER}	Standard deviation associated with spatially correlated geometric rotation errors
λ_{ER}	Length scale parameter associated with the spatially correlated geometric rotation errors
P	Probing effects
σ_{P_0}	Standard uncertainty in the probe radius
σ_P	Standard deviation associated with spatially correlated probing effects
λ_P	Length scale parameter associated with the spatially correlated probing effects

Table 2. Notation associated with the variance matrices; see Section 2. The symbol $A|B$ can be read as 'A, given B'.

Symbol	Association, Interpretation
V_A	variance matrix associated with quantities labelled 'A' due to all influence factors
$V_{A\|B}$	variance matrix associated with quantities labelled 'A' due to influence factors labelled 'B'
K_B	variance factor of V_B with $V_B = K_B K_B^\top$
$G_{A\|B}$	sensitivity matrix of quantities labelled 'A' with respect to influence factors labelled 'B'

2. The GUM Methodology and CMM Point Clouds

2.1. Summary of the Gum Methodology

The uncertainty evaluation approach described in this paper is based on the methodology described in the Guide to the Expression of Uncertainty in Measurement, the GUM, [3], specifically GUM Supplement 2 [10], which deals with multivariate outputs. A feature that distinguishes coordinate metrology from other areas of metrology is the fact that the measurands are usually multivariate, for example, a set of point coordinates, or are derived from multivariate quantities, e.g., the radius of a cylinder associated with a set of coordi-

nates. The GUM methodology involves an input–output model in which the measurand(s) $\boldsymbol{x}$ are described as having a functional relationship $\boldsymbol{x} = \boldsymbol{f}(\boldsymbol{b})$ on a set of inputs or *influence factors* $\boldsymbol{b}$. Any statistical characterisation of the influence factors $\boldsymbol{b}$ defines a corresponding statistical characterisation of the outputs $\boldsymbol{x}$. In particular, if $\boldsymbol{b}$ is associated with a (multivariate) probability distribution with mean $\hat{\boldsymbol{b}}$ and variance matrix V_B, the mean $\hat{\boldsymbol{x}}$ and variance matrix V_X associated with $\boldsymbol{x}$ are completely defined by the functional relationship $\boldsymbol{x} = \boldsymbol{f}(\boldsymbol{b})$. If $\boldsymbol{f}$ is a nonlinear function of $\boldsymbol{b}$, the mean and variance associated with $\boldsymbol{x}$ may be difficult to compute exactly but can be approximated by linearising $\boldsymbol{f}$ about $\hat{\boldsymbol{b}}$. If $G_{X|B}$ is the *sensitivity matrix* of $\boldsymbol{x}$ with respect to $\boldsymbol{b}$,

$$G_{X|B}(i,j) = \frac{f_i}{b_j} \tag{1}$$

then the law of propagation of uncertainty (LPU, [24]) states that $\hat{\boldsymbol{x}}$ and V_X are approximated by

$$\hat{\boldsymbol{x}} \approx \boldsymbol{f}(\hat{\boldsymbol{b}}), \quad V_X \approx G_{X|B} V_B G_{X|B}^{\top}, \tag{2}$$

a multivariate version of the well-known formula used in the GUM. The standard uncertainties $u(\boldsymbol{x})$ associated with $\hat{\boldsymbol{x}}$ are given by the square roots of the diagonal elements of V_X.

If the inputs $\boldsymbol{b}$ are associated with a multivariate Gaussian distribution $\boldsymbol{b} \sim \mathcal{N}(\hat{\boldsymbol{b}}, V_B)$, then the distribution associated with $\boldsymbol{x}$ is approximated by $\mathcal{N}(\hat{\boldsymbol{x}}, V_X)$. Here and elsewhere, the symbol $\sim$ can be read as 'is distributed according to'. The LPU is exact for linear functions $\boldsymbol{f}$ and, for linear $\boldsymbol{f}$, if $\boldsymbol{b}$ is associated with a Gaussian distribution, then $\boldsymbol{x}$ is also associated with the given Gaussian distribution and no approximation is involved. For measurements that are associated with a number of influence factors, the distribution $\mathcal{N}(\hat{\boldsymbol{x}}, V_X)$ is usually a suitable approximation to the true distribution.

The Monte Carlo method (MCM, [9]) for uncertainty evaluation can be used as an alternative to the the LPU approach. The Monte Carlo approach involves assigning distributions to the influence factors $\boldsymbol{b}$, sampling at random $\boldsymbol{b}_q$, $q = 1, \ldots, M$, from these distributions and then evaluating $\boldsymbol{x}_q = \boldsymbol{f}(\boldsymbol{b}_q)$. Then, $\boldsymbol{x}$ is estimated by the mean of the $\boldsymbol{x}_q$ and the associated standard uncertainty is given by standard deviation of the sampled $\boldsymbol{x}_q$. The Monte Carlo method is particularly appropriate if input–output function $\boldsymbol{f}$ is significantly nonlinear. In coordinate metrology, relative accuracies are of the order of 1 part in 10^5 so that second order effects are of the order of 1 part in 10^{10} and can be ignored in almost all applications. This means that the linearisation of $\boldsymbol{f}$ in Equation (2) used to propagate the uncertainty information introduces no significant approximation error. The fact that CMM measurement is subject to a large number of influence factors also implies, through the central limit theorem, that the distributions associated with the measurands are approximated well by Gaussian distributions. Since Gaussian distributions are determined solely by their means and variances, the LPU method provides the essential information about the measurands.

2.2. A GUM Methodology Applied to CMM Measurement

Applying the GUM methodology to CMM measurement requires the following:

- Specifying the set of factors $\boldsymbol{b}$ that influence the measurand(s) $\boldsymbol{x}$.
- Establishing the functional relationship $\boldsymbol{x} = \boldsymbol{f}(\boldsymbol{b})$ that describes how $\boldsymbol{x}$ depends on the influence factors $\boldsymbol{b}$,
- Assigning estimates $\hat{\boldsymbol{b}}$ of the influence factors $\boldsymbol{b}$ and the associated variance matrix V_B.
- Evaluating the sensitivity matrix $G_{X|B}$ given by Equation (1) of $\boldsymbol{x}$ with respect to the influence factors $\boldsymbol{b}$.

Once these steps have been completed, the LPU can be used to provide a statistical characterisation of $\boldsymbol{x}$ in terms of $\hat{\boldsymbol{x}}$ and V_X as in Equation (2).

2.3. A General Model of CMM Measurement

A general model of CMM measurement has the form

$$\boldsymbol{x}_i = \boldsymbol{x}_i^* + \boldsymbol{e}_i + \boldsymbol{\epsilon}_i, \quad \boldsymbol{\epsilon}_i \in \mathcal{N}(\boldsymbol{0}, \sigma_i^2 I) \tag{3}$$

where $\boldsymbol{x}_i$ is the measured coordinates, $\boldsymbol{x}_i^*$ is the true point coordinates, $\boldsymbol{e}_i$ is a systematic effect, and $\boldsymbol{\epsilon}_i$ is a random effect, $i = 1, \ldots, m$. In (3) and elsewhere, the symbol $\in$ can be read as 'is drawn and random from'. The systematic effect $\boldsymbol{e}_i$ is taken to be approximately constant over the duration of a measurement of a part, while the random effect $\boldsymbol{\epsilon}_i$ represents (a sum of) effects that change over a very short timescale, effectively modelling the repeatability component of the CMM.

We generalise the model in Equation (3) to cater for the possibility that the measurements may be subject to a number of independent systematic effects that combine additively to influence the measurement result, e.g.,

$$\boldsymbol{x}_i = \boldsymbol{x}_i^* + \boldsymbol{e}_{i,B} + \boldsymbol{e}_{i,C} + \boldsymbol{e}_{i,D} + \boldsymbol{\epsilon}_i. \tag{4}$$

We assume that the behaviour of the systematic effects can be described by a statistical model that allows us to calculate (or estimate) the contribution to the variance matrix V_X associated with $\boldsymbol{x}_{1:m}$ from the various effects. We denote by $V_{X|B}$ the variance contribution arising from $\boldsymbol{e}_{1:m,B}$, etc. For the model in Equation (4), the variance matrix V_X can be decomposed as

$$V_X = V_{X|B} + V_{X|C} + V_{X|D} + V_{X|R}.$$

2.4. Propagation of Variances

The law of propagation of uncertainty, the basis of the GUM [3], in its multivariate setting [10] describes how uncertainties associated with the measured coordinates in Equation (4) can be evaluated on the basis of uncertainties associated with the systematic and random effects. Suppose effects $\boldsymbol{e}_{i,B} = \boldsymbol{e}_i(\boldsymbol{b})$, $i = 1, \ldots, m$ are specified by n_B parameters $\boldsymbol{b} = (b_1, \ldots, b_{n_B})^\top$ and that a statistical model for $\boldsymbol{b}$ specifies the $n_B \times n_B$ variance matrix V_B associated with $\boldsymbol{b}$. If $G_{X|B}$ is the $3m \times n_B$ sensitivity matrix of $\boldsymbol{x}_{1:m}$ with respect to $\boldsymbol{b}$ constructed from $3 \times n_B$ matrices

$$G_{X|B,i} = \frac{\partial \boldsymbol{x}_i}{\partial \boldsymbol{b}^\top},$$

then

$$V_{X|B} = G_{X|B} V_B G_{X|B}^\top.$$

If V_B can be factored using an eigenvalue decomposition or Cholesky decomposition [25], for example, as $V_B = K_B K_B^\top$ where K_B is an $n_P \times p_B$ matrix (usually $p_B = n_B$), then $V_{X|B}$ can be factored as

$$V_{X|B} = K_{X|B} K_{X|B}^\top, \quad K_{X|B} = G_{X|B} K_B.$$

The role of the sensitivity matrix $G_{X|B}$ can be explained as follows. If the parameters $\boldsymbol{b}$ describing the systematic effects are perturbed by $\Delta\boldsymbol{b}$, then the resulting perturbation on $\boldsymbol{e}_{1:m}$, and hence, $\boldsymbol{x}_{1:m}$, is given by $\Delta\boldsymbol{x}_{1:m} = G_{X|B}\Delta\boldsymbol{b}$ to the first order. Often we are interested in quantities derived from a set of point coordinates. As a consequence of the chain rule in calculus, if $\boldsymbol{a} = (a_1, \ldots, a_{n_A})^\top$ depends on $\boldsymbol{x}_{1:m}$, and $G_{A,X}$ is the $n_A \times 3m$ sensitivity matrix

of $\boldsymbol{a}$ with respect to $\boldsymbol{x}_{1:m}$; then, the $n_A \times n_B$ sensitivity matrix $G_{A|B}$ of A with respect to influence factors $\boldsymbol{b}$ is given by

$$G_{A|B} = G_{A|X} G_{X|B}, \tag{5}$$

and the $n_A \times n_A$ variance matrix $V_{A|B}$ describing the variance contribution to $\boldsymbol{a}$ arising from factors $\boldsymbol{b}$ is given by

$$V_{A|B} = G_{A|B} V_B G_{A|B}^{\top} = K_{A|B} K_{A|B}^{\top}, \quad K_{A|B} = G_{A|B} K_B.$$

If the systematic effects $\boldsymbol{b}$ are perturbed by $\Delta\boldsymbol{b}$, then the derived parameters $\boldsymbol{a}$ are perturbed by $\Delta\boldsymbol{a} = G_{A|B}\Delta\boldsymbol{b}$ to the first order.

This paper considers the following CMM influence factors:

- Repeatability effects (R)
- Probe qualification/location effects (PQ)
- Scale and squareness effects (S)
- Kinematic/geometrical errors: straightness errors (ET)
- Kinematic/geometrical errors: angular/rotation errors (ER)
- Probing effects: probe radius, errors depending on probing direction (P)

The labels in brackets are used consistently in this paper to denote the corresponding influence factor. Temperature effects are assumed to arise via changes in scale and machine geometry. Influence factors arising from software used in coordinate metrology are also extremely important [26] but are not considered further here.

In this paper, we concentrate on the evaluation point cloud uncertainties involving sensitivity matrices $G_{X|B}$ and the uncertainties associated with the distance between pairs of points, a simple but important derived feature. The case of Gaussian-associated features is considered in [27] and shows how the sensitivity matrices $G_{A|X}$ for parameters associated with geometric elements with respect to point cloud data can be calculated. Taken together with the sensitivity matrices $G_{X|B}$ derived in this paper, the sensitivity matrices $G_{A|B}$ can be evaluated as in Equation (5), allowing the uncertainty contribution to the geometric element parameters from each of the influence factors to be evaluated, e.g., the uncertainty associated with the radius of a Gaussian-associated cylinder to squareness errors.

3. Length Measuring Capability and Three-Dimensional Measurement Capability

3.1. Statistical Characterisation and MPE Statements

The MPE statement says that the difference between estimated distance $\hat{d}$ derived from CMM measurement and the true distance d is bounded by a linear function of distance:

$$|\hat{d} - d| \leq A + d/B.$$

The MPE statement for a particular CMM is usually estimated from multiple measurements of calibrated length artefacts [28]. The MPE statement characterises CMM (length measuring) behaviour using two parameters A and B. The MPE statement can be re-interpreted in terms of uncertainty $u(d)$ associated with distance measurement,

$$Ku(d) \leq A + d/B, \tag{6}$$

where K (typically $K = 2$ or $K = 3$) ensures that the probability of exceeding an MPE statement is suitably small. This paper allows us to quantify how the various influence factors contribute to the maximum permissible error. Conversely, an MPE statement can also be used to put bounds on the statistical parameters associated with the modelled

influence factors. For example, a valid MPE statement can be used to bound the size of scale errors associated with a CMM. These issues are considered in detail in Section 6.8. Regarding the MPE statement as a quasi-statistical characterisation of the length measuring capability of a CMM, the MPE statement can also be used to give uncertainty statements for features derived from distances. Such an approach was also considered in the EUCoM project [29].

3.2. Length Measuring Capability Does Not Define Three-Dimensional Measurement Capability

While the length measurement capability of a CMM is clearly important, it is also the case that CMM behaviour is not characterised by length measurement capability alone. In general, length measurement capability provides only limited information about other derived features such as cylindricity, etc. In Section 6.3, it is shown how a combination of independent axes scale effects along with squareness effects provide exactly the same length measuring capability as that arising from a single global scale effect. Therefore, it is possible that two CMMs with exactly the same length measurement capability can perform significantly differently on other measurement tasks, such as the measurement of a ball plate.

3.3. Measurement with a Single Probe Does Not Define Three-Dimensional Measurement Capability

It is also true that complete knowledge of CMM behaviour for a single probe is not sufficient to characterise its behaviour if multiple probes are used. The following example shows that completely characterising the behaviour of a CMM measurement using a single probe offset does not characterise CMM measurements using multiple probes. In particular, experiments to estimate the kinematic errors (see, e.g., [20]) of a CMM must involve multiple probe offsets.

Suppose a CMM has an error behaviour determined by a roll about each axis that depends linearly on the length of travel along the axis. This behaviour can be modelled as

$$\tilde{\boldsymbol{x}} = \boldsymbol{x} + R(\kappa \boldsymbol{x})\boldsymbol{p},$$

where $\boldsymbol{x}$ is the true position of (a fixed point on) the probe assembly, $\boldsymbol{p}$ is the probe offset (from the fixed point), and $\tilde{\boldsymbol{x}}$ is the CMM coordinate measurements (scale readings), R is the linearised rotation matrix corresponding to the roll about each axis given by

$$R(\boldsymbol{x}) = \begin{bmatrix} 1 & -z & y \\ z & 1 & -x \\ -y & x & 1 \end{bmatrix},$$

and $\kappa \approx 0$ is a parameter determining the rate of roll. Then

$$\tilde{\boldsymbol{x}} = \boldsymbol{x} + R(\kappa \boldsymbol{x})\boldsymbol{p} = \boldsymbol{x} + \boldsymbol{p} + \kappa \boldsymbol{x} \times \boldsymbol{p} = R(-\kappa \boldsymbol{p})\boldsymbol{x} + \boldsymbol{p}, \tag{7}$$

where $\boldsymbol{x} \times \boldsymbol{p}$ is the vector cross-product of $\boldsymbol{x}$ with $\boldsymbol{p}$. The relationship Equation (7) shows that measurements of an artefact using a CMM with isotropic axis roll, i.e., having the same rate κ of roll along each axis, are the exact same as those of the same artefact rotated by $R(-\kappa \boldsymbol{p})$ by a CMM with no axis roll (to first order). This equivalence means that, irrespective of measurement strategy and calibration information, a CMM cannot be completely characterised from the multiple measurements of calibrated artefacts such as ball plates and step gauges unless measurements are taken of the same artefact in the same position using more than one probe offset. In general, at least three probe offsets are required; by analogy, the location of three points are needed to track the position of a moving rigid body.

The uncertainty evaluation method described in this paper attempts to characterise fully the three-dimensional nature of CMM measurement with multiple probes.

4. Point Cloud Uncertainty Evaluation: Explicit Models

This section describes models associated with influence factors for which explicit models can be derived directly, enabling the uncertainties associated with these factors to be propagated through to point cloud variance matrices using the law of propagation of uncertainty as in Equation (2).

4.1. Random/Repeatability Component (R)

The simplest model of CMM behaviour is to consider only a random repeatability component constant throughout the working volume:

$$\boldsymbol{x}_i = \boldsymbol{x}_i^* + \boldsymbol{\epsilon}_i, \quad \boldsymbol{\epsilon}_i \in \mathcal{N}(\boldsymbol{0}, \sigma_R^2 I). \tag{8}$$

This model has only one statistical (hyper-)parameter, σ_R. The variance matrix V_X associated with a set of measured coordinates $\boldsymbol{x}_I$ is simply

$$V_X = V_R = \sigma_R^2 I = D_R^2, \quad D_R = \sigma_R I,$$

where I represents the $3m \times 3m$ identity matrix with ones on the diagonal and zeros elsewhere. Despite its simplicity, this model is useful to determine how the uncertainties associated with geometric features depend on representative estimates of the CMM accuracy, as represented by σ_R.

4.2. Probe Qualification Effects (Pq)

For error models with an explicit dependence on the probe offset $\boldsymbol{p}_k$, the fact that the probe configuration geometry is usually determined in probe qualification experiments [30] means that there will be uncertainties associated with estimates of the offsets. If $\boldsymbol{x}_i$ is a measurement using the kth probe, then the uncertainty contribution arising from the probe qualification can be modelled as

$$\boldsymbol{x}_i = \boldsymbol{x}_i^* + \boldsymbol{p}_k + \boldsymbol{e}_{PQ,k} + \boldsymbol{\epsilon}_i, \quad \boldsymbol{e}_{PQ,k} \in \mathcal{N}(\boldsymbol{0}, \sigma_{PQ,k}^2 I), \tag{9}$$

where $\boldsymbol{p}_k$ is the calibrated probe offset vector for the kth probe, and $\boldsymbol{e}_{PQ,k}$ models the difference between the actual probe offset and its calibrated value, $k = 1, \ldots, n_P$. (Model Equation (8) can be regarded as a special case in which the probe offset is $\boldsymbol{p} = \boldsymbol{0}$ and is known exactly.) An important feature of the model is that all measurements with the kth probe are associated with the same systematic effect $\boldsymbol{e}_{PQ,k}$. The variance contribution associated with probe qualification is given by

$$V_{X|PQ} = G_{X|PQ} V_{PQ} G_{X|PQ}^\top$$

where $V_{X|PQ}$ is the $3n_P \times 3n_P$ variance matrix associated with the systematic effects $\boldsymbol{e}_{PQ,k}$, and $G_{X|PQ}$ is the $3m \times 3n_P$ sensitivity matrix. The variance matrix V_{PQ} is a diagonal matrix with the 3×3 matrix $\sigma_{PQ,k}^2 I$ in the kth diagonal block. If the ith measurement is associated with the kth probe, then

$$G_{X|PQ}(3i - 2 : 3i, 3k - 2 : 3k) = I$$

the 3×3 identity matrix, and all other elements in these three rows are zero.

4.3. Scale and Squareness Effects (S)

From practical experience, it is well known that scale and squareness effects are a major component of CMM behaviour. Scale and squareness effects are special cases of a class of models in which the systematic effects in Equation (3) are taken to be functions $\boldsymbol{e}_i = \boldsymbol{e}(\boldsymbol{x}_i, \boldsymbol{b})$ of location $\boldsymbol{x}$ and additional parameters $\boldsymbol{b} = (b_1, \ldots, b_p)^\top$ that model some aspect of CMM behaviour.

The model below incorporates scale effects and three squareness effects through

$$\boldsymbol{x}_i = B(\boldsymbol{b})\boldsymbol{x}_i^*, \tag{10}$$

where

$$B(\boldsymbol{b}) = \begin{bmatrix} (1 + b_{aa} + b_{xx}) & b_{xy} & b_{xz} \\ 0 & (1 + b_{aa} + b_{yy}) & b_{yz} \\ 0 & 0 & (1 + b_{aa} + b_{zz}) \end{bmatrix}$$

depends on effects $\boldsymbol{b} = (b_{aa}, b_{xx}, b_{yy}, b_{zz}, b_{xy}, b_{xz}, b_{yz})^\top$. (The model as it stands assumes the slightly unrealistic case of a zero probe offset). The term b_{aa} models a global scale effect, while b_{xx}, b_{yy} and b_{zz} model scale effects for each axis and b_{xy}, b_{xz} and b_{yz} model the squareness effects. The $3m \times 7$ sensitivity matrix $G_{X|S}$ for this model is assembled from 3×7 matrices of the form

$$G(\boldsymbol{x}_i^*) = \begin{bmatrix} x_i^* & x_i^* & 0 & 0 & y_i^* & z_i^* & 0 \\ y_i^* & 0 & y_i^* & 0 & 0 & 0 & z_i^* \\ z_i^* & 0 & 0 & z_i^* & 0 & 0 & 0 \end{bmatrix}. \tag{11}$$

In practice, $\boldsymbol{x}_i^*$ is unknown but can be approximated accurately by the measured coordinate $\boldsymbol{x}_i$, and the sensitivity matrix is approximated by

$$G_i = G(\boldsymbol{x}_i) = \begin{bmatrix} x_i & x_i & 0 & 0 & y_i & z_i & 0 \\ y_i & 0 & y_i & 0 & 0 & 0 & z_i \\ z_i & 0 & 0 & z_i & 0 & 0 & 0 \end{bmatrix}. \tag{12}$$

The model is completed by specifying the variance matrix V_B associated with the scale and squareness effects, e.g.,

$$V_B = \begin{bmatrix} \sigma_S^2 & 0 & 0 & 0 & 0 & 0 & 0 \\ 0 & \sigma_{S,x}^2 & 0 & 0 & 0 & 0 & 0 \\ 0 & 0 & \sigma_{S,y}^2 & 0 & 0 & 0 & 0 \\ 0 & 0 & 0 & \sigma_{S,z}^2 & 0 & 0 & 0 \\ 0 & 0 & 0 & 0 & \sigma_Q^2 & 0 & 0 \\ 0 & 0 & 0 & 0 & 0 & \sigma_Q^2 & 0 \\ 0 & 0 & 0 & 0 & 0 & 0 & \sigma_Q^2 \end{bmatrix}. \tag{13}$$

If we assume that the individual axis scale effects are associated with the same variance so that $\sigma_{S,x}^2 = \sigma_{S,y}^2 = \sigma_{S,z}^2 = \sigma_{S,a}^2$, the model is associated with four statistical hyper-parameters $\boldsymbol{\sigma} = (\sigma_S, \sigma_{S,a}, \sigma_Q, \sigma_R)^\top$. Given a data point $\boldsymbol{x}_i$, the variance matrix $V_{\boldsymbol{x}_i} = V_{\boldsymbol{x}_i}(\boldsymbol{\sigma})$, due to scale and squareness effects, is given by

$$V_{\boldsymbol{x}_i} = \sigma_S^2 \boldsymbol{x}_i \boldsymbol{x}_i^\top + \begin{bmatrix} x_i^2\sigma_{S,a}^2 + (y_i^2 + z_i^2)\sigma_Q^2 & 0 & 0 \\ 0 & y_i^2\sigma_{S,a}^2 + z_i^2\sigma_Q^2 & 0 \\ 0 & 0 & z_i^2\sigma_{S,a}^2 \end{bmatrix}.$$

For a working volume of $[-L, L]^3$, the variance associated with x-coordinate point $\boldsymbol{x}_L = (L, L, L)^\top$ is $L^2(\sigma_S^2 + \sigma_{S,a}^2 + 2\sigma_Q^2)$, the maximum variance associated with any coordinate in the working volume. This maximum can be compared with statements of maximum permissible error. Over modest working volumes for this model, the variance matrix $V_{X|S}$ associated with a set of coordinates is given by

$$V_{X|S} = G_{X|S} V_S G_{X|S}^\top, \tag{14}$$

where $G_{X|S}$ is the $3m \times 7$ sensitivity matrix constructed from G_i, defined as in Equation (12), and V_S typically has the form in Equation (13).

For measurements involving multiple probe offsets $\boldsymbol{p}_k$, $k = 1, \ldots, n_P$, the measured coordinates $\boldsymbol{x}_i$ are related to the true point coordinates $\boldsymbol{x}_i^*$ through a model of the form

$$\boldsymbol{x}_i = B(\boldsymbol{b})\boldsymbol{x}_i^* + \boldsymbol{p}_{k(i)}.$$

For this model, the sensitivity of $\boldsymbol{x}_i$ with respect to $\boldsymbol{b}$ is approximated by

$$G_i = G(\boldsymbol{x}_i - \boldsymbol{p}_{k(i)})$$

with G defined as in Equation (11).

In two dimensions, the model has the form

$$\boldsymbol{x}_i = \begin{bmatrix} (1 + b_{aa} + b_{xx}) & b_{xy} \\ 0 & (1 + b_{aa} + b_{yy}) \end{bmatrix} \boldsymbol{x}_i^*, \tag{15}$$

depending on effects $\boldsymbol{b} = (b_{aa}, b_{xx}, b_{yy}, b_{xy})^\top$. The $2m \times 4$ sensitivity matrix $G_{X|B}$ for this model is assembled from 2×4 matrices of the form

$$G_i = \begin{bmatrix} x_i & x_i & 0 & y_i \\ y_i & 0 & y_i & 0 \end{bmatrix}, \tag{16}$$

variance matrix V_B associated with the scale and squareness effects typically of the form

$$V_B = \begin{bmatrix} \sigma_S^2 & 0 & 0 & 0 \\ 0 & \sigma_{S,x}^2 & 0 & 0 \\ 0 & 0 & \sigma_{S,y}^2 & 0 \\ 0 & 0 & 0 & \sigma_Q^2 \end{bmatrix}. \tag{17}$$

5. Point Cloud Uncertainty Evaluation: Gaussian Process Error Models

This section considers approximate models for kinematic errors and probing errors based on Gaussian process error models [31,32].

5.1. Model Involving 18 Kinematic Errors

The standard kinematic error model for a CMM [21,33] involves first the specification of 6 error functions associated with the 6 degrees of freedom motion of a rigid body along an axis, e.g., $(e_{xx}(x), e_{xy}, e_{xz}(x), r_{xx}(x), r_{xy}(x), r_{xz}(x))^\top$, where e_{xx} models the scale error along the axis; e_{xy} the straightness error in the xy-plane; and r_{xx} is the rotation about the x-axis, in this case, the roll; $r_{xy}(x)$ is rotation about the y-axis (pitch); and $r_{xz}(x)$ is rotation about the z-axis (yaw). Thus there is a scale error function, two straightness functions and three rotation functions corresponding to roll, pitch and yaw. There are 6 such functions associated with each axis, 18 in all, sometimes augmented by 3 scalar squareness parameters, depending on the convention for specifying the straightness error functions. These error functions are usually modelled in terms of empirical functions such

as polynomials or splines, the coefficients of which are collectively represented by parameter vector $\boldsymbol{b}$. The combined contribution of these 18 + 3 errors to the CMM measurement can be written as

$$\boldsymbol{x}_i = \boldsymbol{x}_i^* + \boldsymbol{e}(\boldsymbol{x}_i^*, \boldsymbol{b}) + R(\boldsymbol{x}_i^*, \boldsymbol{b})\boldsymbol{p}, \tag{18}$$

involving a translation component $\boldsymbol{e}(\boldsymbol{x}_i^*, \boldsymbol{b})$ and a component $R(\boldsymbol{x}_i^*, \boldsymbol{b})$ modelling angular errors where R is a rotation matrix depending on $\boldsymbol{b}$ and location $\boldsymbol{x}^*$. The rotational component also involves the probe offset $\boldsymbol{p}$, the vector pointing from the centre of rotation of the probe housing to the probe tip centre. The explicit dependence on the probe offset allows different probe configurations to be modelled using the same kinematic error functions. Estimates of the function coefficients $\boldsymbol{b}$ along with their associated variance matrix can be determined from repeated measurements of calibrated artefacts such as ball or hole plates [20,34,35].

If V_B is the variance matrix associated with $\boldsymbol{b}$ (derived from a ball plate exercise or otherwise) and $G_{X|B}$ is the sensitivity matrix of $\boldsymbol{x}_{1:m}$ with respect to $\boldsymbol{b}$, then the variance matrix associated with $\boldsymbol{x}_{1:m}$ is given by

$$V_{X|B} = G_{X|B} V_B G_{X|B}^\top.$$

The full kinematic error model and its use in generating variance matrices is very much a specialist undertaking. Typically, each error function is defined in terms of 5 or so parameters, e.g., polynomial coefficients, so that the complete error model involves the order of 100 parameters $\boldsymbol{b}$. Consequently, assigning the associated variance matrix V_B involves estimating the order of 10^4 elements. Below, we consider kinematic error models developed in terms of Gaussian process models that can be specified by a small number of statistical parameters.

5.2. Gaussian Process Models Incorporating Spatial Correlation

Gaussian process (GP) models [32] can be used to develop empirical models of behaviour that do not explicitly involve sets of basis functions such as polynomials or splines. Spatial or temporal correlation associated with data points $(\boldsymbol{x}_i, e_i)$ takes the form $\mathrm{corr}(\mathrm{e}, \mathrm{e}') = k(\boldsymbol{x}, \boldsymbol{x}'|\boldsymbol{\sigma})$ where k is a correlation kernel depending on statistical parameters $\boldsymbol{\sigma}$. Often k depends on $\boldsymbol{x}$ and $\boldsymbol{x}'$ through $\|\boldsymbol{x} - \boldsymbol{x}'\|$, e.g.,

$$\mathrm{cov}(e, e') = k(\boldsymbol{x}, \boldsymbol{x}'|\sigma_E, \lambda_E) = \sigma_E^2 \exp\{-\|\boldsymbol{x} - \boldsymbol{x}'\|^2/\lambda_E^2\}. \tag{19}$$

The strength of the correlation between e and e' depends on the distance between $\boldsymbol{x}$ and $\boldsymbol{x}'$: the closer $\boldsymbol{x}$ is to $\boldsymbol{x}'$, relative to λ, the stronger the correlation between e and e'.

MPE and Spatial Correlation

The use of spatially correlated error models can be motivated in terms of consequences of the statement of maximum permissible error (MPE) in measuring length. In measuring length along a single axis, say the x-axis, suppose the basic statistical model for the measurement of two points is

$$x_1 = x_1^* + e_1 + \epsilon_1, \quad x_2 = x_2^* + e_2 + \epsilon_2,$$

with

$$e_1, e_2 \in \mathcal{N}(0, \sigma_E^2), \quad \epsilon_1, \epsilon_2 \in \mathcal{N}(0, \sigma_R^2).$$

The MPE statement implies that the measured length $\hat{d}_{12}$ is related to the true length d_{12} according to

$$|\hat{d}_{12} - d_{12}| \leq A + d_{12}/B.$$

The MPE implies

$$|e_2 - e_1 + \epsilon_2 - \epsilon_1| \leq A + d_{12}/B$$

so that for $2\sigma_R^2 \leq A^2$ and for $\sigma_R \ll \sigma_E$, the similarity of e_1 and e_2 depends on the *spatial separation* d_{12}.

We can also use a model of the form

$$x = x^* + e(x^*) + \epsilon \approx x^* + e(x) + \epsilon, \quad \epsilon \in \mathcal{N}(0, \sigma_R^2)$$

where $e(x)$ is an error function with $|e(x)| \leq 2\sigma_E$ that encodes the local scale error. (The same concept can be applied to straightness errors, etc.). The MPE implies

$$|e(x_2) - e(x_1) + \epsilon_2 - \epsilon_1| \leq A + |x_2 - x_1|/B$$

so for $\sigma_R \ll \sigma_E$ and $x_1 \neq x_2$,

$$\left| \frac{e(x_2) - e(x_1)}{x_2 - x_1} \right| \leq \frac{A}{|x_2 - x_1|} + \frac{1}{B}.$$

In other words, the slope of the error function $e(x)$ cannot be too large, and so some measure of smoothness on the error function $e(x)$ is required in order for it to be consistent with the MPE statement. From this point of view, in the MPE statement, A quantifies effects over short length scales, while d/B controls the size and smoothness of effects over longer length scales.

Figures 1–3 give examples of spatially correlated error functions generated using the correlation kernel in Equation (19) with $\sigma_E = 0.005$ mm and $\lambda_E = 1000$ mm, 500 mm, 200 mm and 100 mm. These error functions were evaluated at 200 equally spaced points $0 < x_i < 1000$. Given $\boldsymbol{x}$, σ_E and λ_E, each error function is a random draw from the distribution $\mathcal{N}(\mathbf{0}, V(\boldsymbol{x}|\sigma_E, \lambda_E)$, where $V(\boldsymbol{x}|\sigma_E, \lambda_E)$ is the spatially correlated variance matrix. Each error function was centred so that $e(x = 0) = 0$, simulating the convention that the error at $x = 0$ is zero. Each error function represents plausible behaviour, given the spatial correlation. The spatial correlation length λ_E controls the degree of smoothness of the error functions.

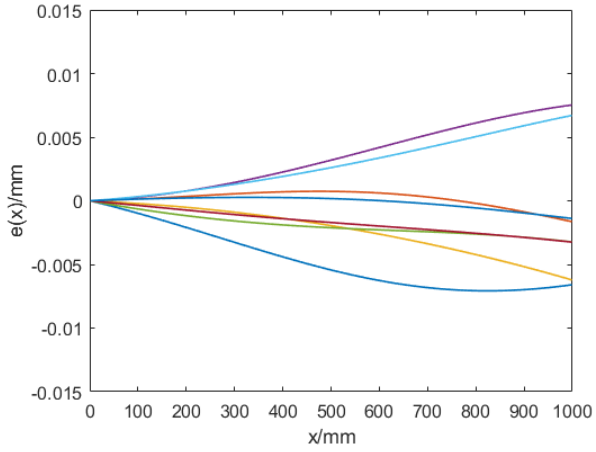

Figure 1. Eight examples of spatially correlated error functions generated using the correlation kernel in Equation (19) with $\sigma_E = 0.005$ mm and $\lambda_E = 1000$ mm. (The colours associated with the functions have no significance.)

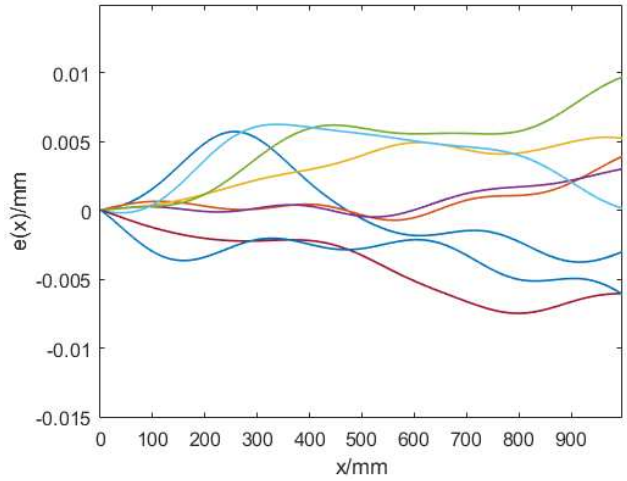

Figure 2. As Figure 1 but with $\lambda_E = 200$ mm.

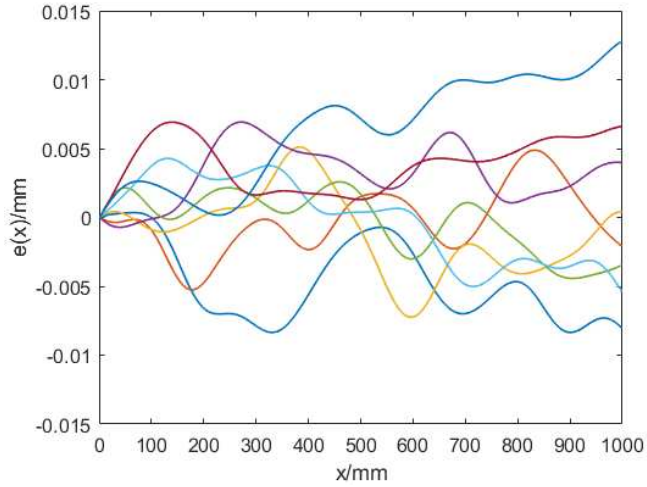

Figure 3. As Figure 1 but with $\lambda_E = 100$ mm.

A GP model can be used to supplement a parametric model $\boldsymbol{e}(\boldsymbol{b})$ for the systematic effects [36], e.g., a scale and squareness error model considered in Section 4.3 in which the role of the GP model is to simulate behaviour not captured by the parametric model, such as uncorrected kinematic errors. The significant advantage of GP models is that they can mimic the behaviour of empirical models in a non-parametric way and can be defined by a small number of statistical parameters. The point cloud variance matrices V_X can be constructed from the point cloud coordinates $\boldsymbol{x}_{1:m}$, along with a few statistical parameters. In the models below, the geometric location errors, rotational errors and probing errors can each be modelled by specifying only two statistical parameters each. By contrast, kinematic error models, Section 5.1, typically involve 100 or so parameters.

5.3. Gaussian Models for Location Errors (ET)

We can apply a GP model for CMM behaviour, as follows, with

$$\boldsymbol{x}_i = \boldsymbol{x}_i^* + \boldsymbol{e}_i, \tag{20}$$

where the systematic effects are spatially (and sometimes temporally) correlated with the systematic effects $\boldsymbol{e}_i$. In general, the covariance applies only to the same coordinates,

with the x-, y- and z-coordinates of $\boldsymbol{e}$ mutually independent. The covariance of e_x with e'_x could be modelled as

$$\mathrm{cov}(e_x, e'_x) = k(\boldsymbol{x}, \boldsymbol{x}'|\sigma_{ET,x}, \lambda_{ET,x}) = \sigma^2_{ET,x} \exp\Big\{-\|\boldsymbol{x} - \boldsymbol{x}'\|^2/\lambda^2_{ET,x}\Big\}, \tag{21}$$

for example, where $\lambda_{ET,x}$ defines the length scale for the correlation in the x-coordinate. Note that in this model, the strength of the correlation in the effects e_x depends on the distance $\|\boldsymbol{x} - \boldsymbol{x}'|$ in 3D, not the distance along the x-axis.

Let D be the $m \times m$ matrix of distances with $D_{ij} = \|\boldsymbol{x}_i - \boldsymbol{x}_j\|$. The variance contribution V_{XT} from $\boldsymbol{e}_{1:m}$ to the x-coordinates of $\boldsymbol{x}_{i:m}$ is given by

$$V_{XT,x} = \sigma^2_{ET,x} \exp\Big\{-D^2/\lambda^2_{ET,x}\Big\},$$

where the calculations associated with D are made element-wise. The contribution to the y- and z-components are of exactly the same form. The matrix V_{XT} is assembled from $V_{XT,x}$ $V_{XT,y}$ and $V_{XT,z}$, with all other elements zeros since we assume that the systematic effects associated with the x-coordinates are independent from those associated with the y- and z-coordinates. We assume that the GP model relates to uncorrected kinematic errors that are not likely to have a significant correlation between axes, even if the kinematic errors themselves are likely to produce such a correlation. While the GP model assumes there is no inter-axes correlation, the GP model will model successful behaviour that does have such a correlation.

If it can be assumed that the systematic effects along each axis have the same behaviour, so that $\sigma_{ET,x} = \sigma_{ET,y} = \sigma_{ET,z} = \sigma_{ET}$, etc., then the model is specified by two statistical hyper-parameters σ_{ET} and λ_{ET}.

Gaussian Process Models for Location Errors Incorporating Multiple Probes

Suppose that the point cloud $\boldsymbol{x}_{1:m}$ is gathered using multiple probes with offsets $\boldsymbol{p}_k$, $k = 1, \ldots, n_P$. The measured coordinates $\boldsymbol{x}_i$ are related to the true point coordinates $\boldsymbol{x}^*_i$ through a model of the form

$$\boldsymbol{x}_i = \boldsymbol{x}^*_i + \boldsymbol{e}_i + \boldsymbol{p}_{k(i)} + \boldsymbol{\epsilon}_i,$$

where $\boldsymbol{p}_{k(i)}$ denotes the probe configuration associated with the ith measurement, etc. For this case, it is important to note that the spatial correlation is dependent on $\|\boldsymbol{x}^*_i - \boldsymbol{x}^*_j\|$, not $\|\boldsymbol{x}_i - \boldsymbol{x}_j\|$. For different probe configurations, we have

$$\|\boldsymbol{x}^*_i - \boldsymbol{x}^*_j\| \doteq \|(\boldsymbol{x}_i - \boldsymbol{p}_{k(i)}) - (\boldsymbol{x}_j - \boldsymbol{p}_{k(j)})\|.$$

Similar considerations apply to the model for scale and squareness errors with multiple probe offsets, Section 4.3, and for GP models for rotation errors, Section 5.4, below.

5.4. Gaussian Process Models for Rotation Errors (Er)

The GP models in Section 5.3 used, perhaps, with a simple parametric error model can simulate a wide range of plausible CMM behaviour, but it relates only to one probing configuration and does not, without modification, allow us to evaluate the uncertainties associated with different probe configurations. An extension of the model is to use GP models to model both the location and rotation errors:

$$\boldsymbol{x}_i = \boldsymbol{x}^*_i + \boldsymbol{e}_i + R(\boldsymbol{\alpha}_i)\boldsymbol{p} + \boldsymbol{\epsilon}_i, \tag{22}$$

where $\boldsymbol{\alpha}_i = (\alpha_{i,x}, \alpha_{i,y}, \alpha_{i,z})^\top$ represents three spatially correlated rotation errors acting on the probe offset vector $\boldsymbol{p}$ through the rotation matrix

$$R(\boldsymbol{\alpha}_i) = R_z(\alpha_{i,z})R_y(\alpha_{i,y})R_x(\alpha_{i,x}), \tag{23}$$

the product of rotations about each of the three coordinate axes:

$$R_x(\alpha_x) = \begin{bmatrix} 1 & 0 & 0 \\ 0 & \cos\alpha_x & -\sin\alpha_x \\ 0 & \sin\alpha_x & \cos\alpha_x \end{bmatrix}, \quad R_y(\alpha_y) = \begin{bmatrix} \cos\alpha_y & 0 & \sin\alpha_y \\ 0 & 1 & 0 \\ -\sin\alpha_y & 0 & \cos\alpha_y \end{bmatrix},$$

and

$$R_z(\alpha_z) = \begin{bmatrix} \cos\alpha_z & -\sin\alpha_z & 0 \\ \sin\alpha_z & \cos\alpha_z & 0 \\ 0 & 0 & 1 \end{bmatrix}.$$

We assume that the rotational effects about one axis are independent from the rotational effects about the other two axes, but other more general approaches are possible. For measurements involving multiple probes, the degree of spatial correlation associated with $\boldsymbol{\alpha}_i$ and $\boldsymbol{\alpha}_j$ depends on

$$\|\boldsymbol{x}_i^* - \boldsymbol{x}_j^*\| \doteq \|(\boldsymbol{x}_i - \boldsymbol{p}_{k(i)}) - (\boldsymbol{x}_j - \boldsymbol{p}_{k(j)})\|.$$

If the rotational errors are similar along each axis, then the GP model for the rotational errors is specified by the two statistical hyper-parameters σ_{ER}, and λ_{ER}.

The variance associated with location errors for any coordinate is σ_{ET}^2. If the maximum probe length is P, then the maximum variance associated with rotational effects for a coordinate is given by $P^2\sigma_{ER}^2$. Hence, the maximum variance associated with location and rotation errors for a coordinate is given by $\sigma_{ET}^2 + P^2\sigma_{ER}^2$. This maximum can be compared with statements of maximum permissible error.

We note that if the variance matrix associated with $\boldsymbol{\alpha} = (\alpha_x, \alpha_y, \alpha_z)^\top$ with $\boldsymbol{\alpha} = \mathbf{0}$ is $V_{\boldsymbol{\alpha}}$, then the variance matrix $V_{\boldsymbol{p}}$ associated with $R(\boldsymbol{\alpha})\boldsymbol{p}$, with $R(\boldsymbol{\alpha})$ as in Equation (23), is given by $GV_{\boldsymbol{\alpha}}G^\top$, where

$$G = \begin{bmatrix} 0 & p_z & -p_y \\ -p_z & 0 & p_x \\ p_y & -p_x & 0 \end{bmatrix}, \quad \boldsymbol{p} = (p_x, p_y, p_z)^\top. \tag{24}$$

As for the case of the kinematic error model, the explicit dependence on the probe offset allows for the uncertainty contributions for different probe configurations to be taken into account.

If V_{AR} is the $3m \times 3m$ variance matrix associated with $\boldsymbol{\alpha}_{1:m}$ determined from the correlation kernel (or otherwise), then the variance contribution V_{XR} to the measurements $\boldsymbol{x}_{1:m}$ is given by

$$V_{XR} = G_{XR}V_{AR}G_{XR}^\top,$$

where G_{XR} is a $3m \times 3m$ block-diagonal matrix. If the ith measurement is associated with the kth probe, then the 3×3 ith diagonal is equal to G_k, where G_k is constructed from $\boldsymbol{p}_k$ as in Equation (24). Although the model for the rotation angles about the three axes are mutually independent, the sensitivity matrices G_{XR} in general will introduce correlation between the effects applied to the x-, y- and z-coordinates.

If the variances and spatial correlation lengths are the same for each axis and equal to σ_{ER}^2 and λ_{ER}, respectively, then the variance matrix V_{XR} is constructed from 3×3 blocks of the form

$$V_{ij} = \sigma_{ER}^2\left(\exp^{-d_{ij}^2/\lambda_{ER}^2}\right)G_{k(i)}G_{k(j)}^\top, \tag{25}$$

where G_k is defined as in Equation (24) involving the two statistical hyper-parameters σ_{ER} and λ_{ER}.

5.5. Gaussian Process Models for Probing Effects (P)

The operation of the probe system will also make a variance contribution. While the CMM geometric errors are likely to vary smoothly with location, the probing errors are likely to vary smoothly with probing direction where the probing direction is usually designed to be normal to the surface being probed. We can augment the model in Equation (20) to one of the form

$$\boldsymbol{x}_i = \boldsymbol{x}_i^* + \boldsymbol{e}_i + (e_{P,0} + e_{P,i})\boldsymbol{n}_i + \boldsymbol{\epsilon}_i, \tag{26}$$

where $e_{P,0}$ is a fixed offset representing the uncertainty in the estimate of the probe radius, $e_{P,i}$ is a spatially correlated systematic effect associated with probing, and $\boldsymbol{n}_i$ is the unit normal probing direction. The correlation between effects $e_{P,i}$ and $e_{P,j}$ depends on the spatial separation $\|\boldsymbol{n}_i - \boldsymbol{n}_j\|$ if both measurements are made using the same probe. The angular distance between $\boldsymbol{n}_i$ and $\boldsymbol{n}_j$ may seem a more natural distance between two unit vectors but can lead to matrices that are not positive (semi-)definite, i.e., they have negative eigenvalues and are therefore not admissible as variance matrices. Similar issues arise in applying GP models on other surfaces such as a cylinder. There are strong constraints on measures of distance that can be used to specify spatial correlation; see, e.g., [37]. Using the Euclidean distance, i.e., the distance in 3-dimensions, always leads to admissible variance matrices.

We assume that the probing effects associated with different probes are statistically independent (although there may be situations where some statistical dependence would be expected). We assume that $e_{P,0}$ is associated with variance $\sigma_{P_0}^2$ and $\boldsymbol{e}_{P,i}$ with variance σ_P^2 and length scale parameter λ_P. If V_{DP} is given by

$$V_{DP}(i,j) = \sigma_{P_0}^2 + \sigma_P^2 e^{-d_{P,ij}^2/\lambda_P^2}, \quad d_{P,ij} = \|\boldsymbol{n}_j - \boldsymbol{n}_i\|, \tag{27}$$

then the variance contribution V_{XP} associated with probing effects is given by

$$V_{XP} = NV_{DP}N^\top$$

where N is the $3m \times m$ block diagonal matrix with $\boldsymbol{n}_i$ in the ith diagonal block.

5.6. Combining Effects

We can write the point cloud variance matrix V_X incorporating all the effects considered above as

$$V_X = V_{XT} + V_{XR} + V_{XP} + G_{X|PQ}V_{PQ}G_{X|PQ}^\top + G_{X|S}V_SG_{X|S}^\top + V_R, \tag{28}$$

where the first three variance matrices on the right hand side are derived from spatially correlated location, rotation and probing effects and the second three are the contributions from probe qualification effects, scale and squareness effects and independent random effects, respectively. For some cases, not all effects need to be considered. For example, for measurements using a single probe, rotational effects and probe qualification effects need not be calculated. While the model does have some degree of complexity, all the variance matrices can be calculated using direct calculations based on, for example, the point coordinates, the distances between points, etc. All calculations have been implemented in spreadsheets, for example.

If $G_{A|X}$ is the sensitivity matrix associated with a feature vector $\boldsymbol{a}$ with respect to coordinates $\boldsymbol{x}_{1:m}$, then the variance matrix V_A associated with $\boldsymbol{a}$ can also be decomposed as

$$\begin{aligned} V_A =& V_{A|XT} + V_{A|XR} + V_{A|XP} + \ldots \\ & G_{A|PQ} V_{PQ} G_{A|PQ}^\top + G_{A|S} V_B G_{A|S}^\top + G_{A|X} V_R G_{A|X}^\top, \end{aligned}$$

where $V_{A|XT} = G_{A|X} V_{XT} G_{A|X}^\top$, etc., and $G_{A|S} = G_{A|X} G_{X|S}$, etc. Thus, $G_{A|PQ} V_{PQ} G_{A|PQ}^\top$ is the variance contribution to V_A arising from probe qualification effects, for example.

The uncertainty contributions to $u(\boldsymbol{a})$ from each of the influence factors can also be evaluated:

$$u^2(\boldsymbol{a}) = u_{ET}^2(\boldsymbol{a}) + u_{ER}^2(\boldsymbol{a}) + u_P^2(\boldsymbol{a}) + u_{PQ}^2(\boldsymbol{a}) + u_S^2(\boldsymbol{a}) + u_R^2(\boldsymbol{a}),$$

where $u_{ET}^2(\boldsymbol{a})$ is the set of diagonal elements of $V_{A|XT}$, etc.

6. Uncertainties Associated with Distances Derived from Point Clouds

This section considers how uncertainties associated with a point cloud can be propagated through to the uncertainties associated with the distance between pairs of points.

If a model determines the point cloud matrices $V_X(\boldsymbol{\sigma})$ associated with $\boldsymbol{x}_{i:m}$ in terms of statistical parameters $\boldsymbol{\sigma}$, then for any pair of points $\boldsymbol{x}_i$ and $\boldsymbol{x}_j$, we can calculate the variance associated with the distance d_{ij} according to

$$u^2(d_{ij}) = \begin{bmatrix} \boldsymbol{n}_{ij} \\ -\boldsymbol{n}_{ij} \end{bmatrix}^\top V_{ij} \begin{bmatrix} \boldsymbol{n}_{ij} \\ -\boldsymbol{n}_{ij} \end{bmatrix}, \quad \boldsymbol{n}_{ij} = \frac{1}{d_{ij}}(\boldsymbol{x}_i - \boldsymbol{x}_j) \tag{29}$$

where V_{ij} is the 6×6 variance matrix formed from the $3i-2:3i$th and $3j-2:3j$th rows and columns of V_X. The uncertainty contribution from each of the influence factors can also be derived from the variance decomposition in Equation (28):

$$u^2(d_{ij}) = u_{ET}^2(d_{ij}) + u_{ER}^2(d_{ij}) + u_P^2(d_{ij}) + u_{PQ}^2(d_{ij}) + u_S^2(d_{ij}) + u_R^2(d_{ij}). \tag{30}$$

Often we are interested in the difference in distances, e.g., in comparing the distance associated with a test artefact with that associated with a calibrated reference artefact. Differences in distances also come into the impact of CMM uncertainties in form errors, e.g., the uncertainties associated with the difference in two diameters of a spherical or cylindrical artefact. Using the same notation,

$$u^2(d_{ij} - d_{rs}) = \begin{bmatrix} \boldsymbol{n}_{ij} \\ -\boldsymbol{n}_{ij} \\ -\boldsymbol{n}_{rs} \\ \boldsymbol{n}_{rs} \end{bmatrix}^\top V_{ijrs} \begin{bmatrix} \boldsymbol{n}_{ij} \\ -\boldsymbol{n}_{ij} \\ -\boldsymbol{n}_{rs} \\ \boldsymbol{n}_{rs} \end{bmatrix},$$

where V_{ijrs} is the 12×12 variance matrix formed from relevant rows and columns of V_X.

6.1. Distance Measurement: Uncertainty Contribution Associated with Random Effects

If $V_X = \sigma_R^2 I$, then

$$u^2(d_{ij}) = 2\sigma_R^2.$$

If $d_{ij} = \|\boldsymbol{x}_j - \boldsymbol{x}_i\|$ and $d_{rs} = \|\boldsymbol{x}_s - \boldsymbol{x}_r\|$, then

$$u^2(d_{ij} - d_{rs}) = 4\sigma_R^2.$$

Note that these uncertainties depend only on σ_R and are independent of location and separation of the points.

6.2. Distance Measurement: Uncertainty Contribution from Probe Qualification Effects

We assume that probe qualification effects are modelled as in Section 4.2:

$$\boldsymbol{e}_{PQ,k} \in \mathcal{N}(\mathbf{0}, \sigma^2_{PQ,k} I).$$

If $\boldsymbol{x}_i$ and $\boldsymbol{x}_j$ are measured using the same probe, then the uncertainty contribution to the distance d_{ij} from probe qualification effects is zero. Otherwise,

$$u^2(d_{ij}) = \sigma^2_{PQ,k(i)} + \sigma^2_{PQ,k(j)}.$$

The uncertainty contribution associated with $d_{ij} - d_{rs}$ arises from the term

$$(\boldsymbol{e}_{k(i)} - \boldsymbol{e}_{k(j)})^\top \boldsymbol{n}_{ij} - (\boldsymbol{e}_{k(r)} - \boldsymbol{e}_{k(s)})^\top \boldsymbol{n}_{rs}.$$

If $k(i) = k(j)$ and $k(r) = k(s)$, then $u^2(d_{ij} - d_{rs}) = 0$. If $k(r) = k(s)$ but $k(i) \neq k(j)$, then

$$u^2(d_{ij} - d_{rs}) = u^2(d_{ij}) = \sigma^2_{PQ,k(i)} + \sigma^2_{PQ,k(j)}.$$

If $k(i) = k(r)$ and $k(j) = k(s)$ but $k(i) \neq k(j)$, then

$$u^2(d_{ij} - d_{rs}) = (2 - 2\boldsymbol{n}_{ij}^\top \boldsymbol{n}_{rs}) \left(\sigma^2_{PQ,k(i)} + \sigma^2_{PQ,k(j)} \right),$$

so that

$$0 \leq u^2(d_{ij} - d_{rs}) \leq 4 \left(\sigma^2_{PQ,k(i)} + \sigma^2_{PQ,k(j)} \right),$$

depending on the angle between $\boldsymbol{n}_{ij}$ and $\boldsymbol{n}_{rs}$. The uncertainty contribution is zero if $\boldsymbol{n}_{ij} = \boldsymbol{n}_{rs}$, e.g., when two gauge blocks are measured parallel to each other with both left faces measured by one probe and both right faces by the other. The uncertainty contribution is maximised when $\boldsymbol{n}_{ij} = -\boldsymbol{n}_{rs}$, e.g., when the left face of one gauge block is measured by one probe and the left face of a second parallel gauge block is measured by the other probe with the probes interchanged for the right face. If all four measurements are undertaken by different probes, then

$$u^2(d_{ij} - d_{rs}) = u^2(d_{ij}) + u^2(d_{rs}) = \sigma^2_{PQ,k(i)} + \sigma^2_{PQ,k(j)} + \sigma^2_{PQ,k(r)} + \sigma^2_{PQ,k(s)}.$$

6.3. Distance Measurement: Uncertainty Contribution Associated with Scale and Squareness Effects

We consider scale and squareness model as in Equation (10), involving seven random effects $\boldsymbol{b} = (b_{aa}, b_{xx}, b_{yy}, b_{zz}, b_{xy}, b_{xz}, b_{yz})^\top$. Given two data points $\boldsymbol{x}_i$ and $\boldsymbol{x}_j$, let $d_{ij} = \|\boldsymbol{x}_j - \boldsymbol{x}_i\|$ and $x_{ij} = x_j - x_i$, $y_{ij} = y_j - y_i$ and $z_{ij} = z_j - z_i$. Then the 1×7 sensitivity matrix $G_{D|ij}$ of d_{ij} with respect to the scale and squareness effects $\boldsymbol{e}$ is given by

$$G_{D|ij} = \frac{1}{d_{ij}} \begin{bmatrix} d_{ij}^2 & x_{ij}^2 & y_{ij}^2 & z_{ij}^2 & x_{ij}y_{ij} & x_{ij}z_{ij} & y_{ij}z_{ij} \end{bmatrix}.$$

(Strictly, $G_{D|ij}$ is the sensitivity matrix of $\delta_{ij} = (\boldsymbol{x}_j - \boldsymbol{x}_i)^\top \boldsymbol{n}_{ij}$ where $\boldsymbol{n}_{ij} = (\boldsymbol{x}_j - \boldsymbol{x}_i)/d_{ij}$. We note that δ_{ij} is a signed quantity with $\delta_{ij} = \pm d_{ij}$). If

$$b_{aa} \sim \mathcal{N}(0, \sigma_S^2), \quad b_{xx}, b_{yy}, b_{zz} \sim \mathcal{N}(0, \sigma_{S,a}^2),$$

and

$$b_{xy}, b_{xz}, b_{yz} \sim \mathcal{N}(0, \sigma_Q^2).$$

then

$$u^2(d_{ij}) = \sigma_S^2 d_{ij}^2 + \sigma_{S,a}^2 D_{S,a}^2 + \sigma_Q^2 D_Q^2, \tag{31}$$

where

$$D_{S,a}^2 = \frac{1}{d_{ij}^2}\left[x_{ij}^4 + y_{ij}^4 + z_{ij}^4\right],$$

and

$$D_Q^2 = \frac{1}{d_{ij}^2}\left[x_{ij}^2 y_{ij}^2 + x_{ij}^2 z_{ij}^2 + y_{ij}^2 z_{ij}^2\right].$$

The expression for $u^2(d_{ij})$ in Equation (31) shows non-isotropic behaviour in that the uncertainty depends not only on the distance but also the position of the points $\boldsymbol{x}_i$ and $\boldsymbol{x}_j$. In particular, if $\boldsymbol{x}_i$ and $\boldsymbol{x}_j$ are aligned with an axis direction, the cross terms $x_{ij}y_{ij}$ are all zero along with two of x_{ij}, y_{ij} and z_{ij}. For this case, $u(d_{ij})$ is given by

$$u^2(d_{ij}) = (\sigma_S^2 + \sigma_{S,a}^2) d_{ij}^2,$$

and does not have a contribution from squareness effects.

If $d_{ij} = \|\boldsymbol{x}_j - \boldsymbol{x}_i\|$ and $d_{rs} = \|\boldsymbol{x}_s - \boldsymbol{x}_r\|$, then

$$u^2(d_{ij} - d_{rs}) = \sigma_S^2 (d_{ij} - d_{rs})^2 + \sigma_{S,a}^2 D_{S,a}^2 + \sigma_Q^2 D_Q^2,$$

where

$$D_{S,a}^2 = \left(\frac{x_{ij}^2}{d_{ij}} - \frac{x_{rs}^2}{d_{rs}}\right)^2 + \left(\frac{y_{ij}^2}{d_{ij}} - \frac{y_{rs}^2}{d_{rs}}\right)^2 + \left(\frac{z_{ij}^2}{d_{ij}} - \frac{z_{rs}^2}{d_{rs}}\right)^2$$

and $D_Q^2 =$

$$\left(\frac{x_{ij}y_{ij}}{d_{ij}} - \frac{x_{rs}y_{rs}}{d_{rs}}\right)^2 + \left(\frac{x_{ij}z_{ij}}{d_{ij}} - \frac{x_{rs}z_{rs}}{d_{rs}}\right)^2 + \left(\frac{y_{ij}z_{ij}}{d_{ij}} - \frac{y_{rs}z_{rs}}{d_{rs}}\right)^2.$$

For example, if $\boldsymbol{x}_1$ and $\boldsymbol{x}_2$ and $\boldsymbol{x}_3$ and $\boldsymbol{x}_4$ are the end points of diameters with $d_{12} = d_{34} = d$, and $\boldsymbol{x}_2 - \boldsymbol{x}_1$ is parallel to the x-axis and $\boldsymbol{x}_4 - \boldsymbol{x}_3$ parallel to the y-axis, then $u^2(d_{12} - d_{34}) = 2d^2\sigma_{S,a}^2$. By contrast, if the four points are rotated by 45°, then $u^2(d_{12} - d_{34}) = \sigma_Q^2 d^2$. If $\boldsymbol{x}_2 - \boldsymbol{x}_1$ is parallel to $\boldsymbol{x}_4 - \boldsymbol{x}_3$ and $d_{12} = d_{34} = d$, then $u^2(d_{12} - d_{34}) = 0$, showing that scale and squareness effects make no significant contribution to the uncertainty in calibrating a test length standard against a reference length standard of nominally the same length if the two standards are aligned parallel to each other.

Two Scale and Squareness Models with the Same Distance Measurement Behaviour

From the expressions for $u^2(d_{ij})$ in Equation (31), we note that if $\sigma_Q^2 = 2\sigma_{S,a}^2 = \tau^2$, say, then

$$\sigma_{S,a}^2 D_{S,a}^2 + \sigma_Q^2 D_Q^2 = \frac{1}{d_{ij}^2}\tau^2 d_{ij}^4 = \tau^2 d_{ij}^2,$$

and so

$$u^2(d_{ij}) = \left(\sigma_S^2 + \tau^2\right) d_{ij}^2.$$

Thus, if $\sigma_Q^2 = 2\sigma_{S,a}^2 = \tau^2$, then the uncertainty associated with the measurement of any distance is exactly the same as for a CMM that has only a single global scale effect with $\tilde{\sigma}_S^2 = \sigma_S^2 + \tau^2$. While the measurement of distance has exactly the same behaviour, the measurement of other features could be quite different. For example, a global scale effect will have little contribution to the measurement of form error of a sphere, while any squareness effect will have a contribution.

This example also shows that it is not possible to characterise the uncertainty contribution of a CMM measurement purely on the basis of an MPE statement.

6.4. Distance Measurement: Uncertainty Contribution from Spatially Correlated Location Effects

See Section 5.3. Suppose that

$$\boldsymbol{x}_i = \boldsymbol{x}_i^* + \boldsymbol{e}_i, \quad \boldsymbol{x}_j = \boldsymbol{x}_j^* + \boldsymbol{e}_j,$$

where $\boldsymbol{e}_i$ and $\boldsymbol{e}_j$ are correlated effects. Suppose the x-components of the correlated effects are such that

$$e_{i,x}, e_{j,x} \sim \mathcal{N}(0, \sigma_x^2),$$

and the coefficient of correlation for these two effects is $\rho_{ij,x}$, and the y- and z-components are similarly distributed. Assuming that the x-, y- and z-components are mutually independent, then

$$u^2(d_{ij}) = \frac{2}{d_{ij}^2}\Big(x_{ij}^2\sigma_x^2(1-\rho_{ij,x}) + y_{ij}^2\sigma_y^2(1-\rho_{ij,y}) + z_{ij}^2\sigma_z^2(1-\rho_{ij,z})\Big).$$

(Here $x_{ij} = x_j - x_i$, etc., as before). If the correlation is described in terms of a correlation kernel as in Equation (21), then $\rho_{ij,x} = e^{-d_{ij}^2/\lambda_x^2}$. If the correlation behaviour is the same in each axis with $\sigma_x = \sigma_y = \sigma_z = \sigma_{ET}$ and $\rho_{ij,x} = \rho_{ij,y} = \rho_{ij,z} = \rho_{ij} = e^{-d_{ij}^2/\lambda_{ET}^2}$, then

$$u^2(d_{ij}) = 2\sigma_{ET}^2\Big(1 - e^{-d_{ij}^2/\lambda_{ET}^2}\Big).$$

Let $r = d_{ij}/\lambda_{ET}$. Then

$$\begin{aligned} 1 - e^{-d_{ij}^2/\lambda_{ET}^2} &= 1 - \left\{1 - r^2 + \frac{r^4}{2!} - \frac{r^6}{3!} + \cdots\right\}, \\ &= r^2 - \frac{r^4}{2!} + \frac{r^6}{3!} - \cdots \end{aligned}$$

If λ_{ET} is much greater than d_{ij}, then e^{-r^2} is close to 1 and the uncertainty is the distance close to zero. For this case, the effects $\boldsymbol{e}_i \approx \boldsymbol{e}_j$ act like a fixed offset associated with the measurements (similar to a probe qualification effect) and do not contribute to the uncertainty associated with the distance. For d_{ij} somewhat less than λ_{ET}, the term on the right above is dominated by the first term r^2 so that

$$u^2(d_{ij}) \approx 2\sigma_{ET}^2\frac{d_{ij}^2}{\lambda_{ET}^2}.$$

In this case, the uncertainty associated with d_{ij} is approximately proportional to d_{ij}, showing that the correlated effects behave somewhat like a scale effect. If d_{ij} is much greater then λ_{ET}, the $e^{-d_{ij}^2/\lambda_{ET}^2} \approx 0$ and

$$u^2(d_{ij}) \approx 2\sigma_{ET}^2.$$

For this case the correlated effects behave more like independent random effects. Figures 1–3 also give insight into the dependence of uncertainties associated with distances on spatial correlation length.

We now evaluate the uncertainty $u(d_{ij} - d_{rs})$ in the difference in two distances associated with four points associated with an isotropic spatial correlation model defined by

statistical parameters σ_{ET} and length scale parameter λ_{ET}. Let $\boldsymbol{n}_{ij}$ be the unit normal point in the direction $\boldsymbol{x}_j - \boldsymbol{x}_i$, and let $\boldsymbol{n}_{rs}$ be defined similarly. Then,

$$u^2(d_{ij} - d_{rs}) = \sigma_{ET}^2 \boldsymbol{g}^\top V_N \boldsymbol{g}, \quad \boldsymbol{g} = (1, -1, -1, 1)^\top,$$

with

$$V_N = \begin{bmatrix} 1 & e^{-d_{ij}^2/\lambda_{ET}^2} & ce^{-d_{ir}^2/\lambda_{ET}^2} & ce^{-d_{is}^2/\lambda_{ET}^2} \\ e^{-d_{ij}^2/\lambda_{ET}^2} & 1 & ce^{-d_{jr}^2/\lambda_{ET}^2} & ce^{-d_{js}^2/\lambda_{ET}^2} \\ ce^{-d_{ir}^2/\lambda_{ET}^2} & ce^{-d_{jr}^2/\lambda_{ET}^2} & 1 & e^{-d_{rs}^2/\lambda_{ET}^2} \\ ce^{-d_{is}^2/\lambda_{ET}^2} & ce^{-d_{js}^2/\lambda_{ET}^2} & e^{-d_{rs}^2/\lambda_{ET}^2} & 1 \end{bmatrix},$$

where $c = \boldsymbol{n}_{ij}^\top \boldsymbol{n}_{rs}$, the cosine of the angle between the two normal vectors. Performing the matrix–vector multiplications, we end up with

$$u^2(d_{ij} - d_{rs}) = 2\sigma_{ET}^2 \big(2 - e_{ij} - e_{rs} + c(e_{jr} + e_{is} - e_{ir} - e_{js})\big),$$

where $e_{ij} = e^{-d_{ij}^2/\lambda_{ET}^2}$, etc.

Example: comparison of two gauge blocks. Suppose two gauge blocks of nominally the sample length are measured side by side, parallel to each other, with $\boldsymbol{x}_1$ and $\boldsymbol{x}_2$ as the measured points on the end faces of the first gauge block and $\boldsymbol{x}_3$ and $\boldsymbol{x}_4$ those corresponding to the second gauge block. For this case, $d_{12} \approx d_{34} = D$, say, $d_{13} \approx d_{24} = d$, say, and $n_{12} \approx n_{34}$ so that $c \approx 1$. If d is much smaller than D, then $d_{14} \approx d_{23} \approx d_{12}$, and

$$u^2(d_{12} - d_{34}) \approx 4\sigma_{ET}^2 \Big(1 - e^{-d^2/\lambda_{ET}^2}\Big).$$

This uncertainty can be thought of as a quantification of the Abbe contribution to the uncertainty due to the fact that the measuring lines associated with the two gauge blocks are displaced by d from each other. For d much smaller than λ_{ET}, this contribution is negligible.

6.5. Distance Measurement: Uncertainty Contribution from Spatially Correlated Rotation Effects

See Section 5.4. We assume the spatial correlation is isotropic, i.e., the same for each axis, and specified by variance σ_{ER}^2 and length scale parameter λ_{ER}. If $\boldsymbol{x}_i$ is measured using probe offset $\boldsymbol{p}_{k(i)}$, etc., $\boldsymbol{n}_{ij}$ is the unit vector pointing from $\boldsymbol{x}_i$ to $\boldsymbol{x}_j$, and G_i and G_j are the sensitivity matrices associated with $R(\boldsymbol{\alpha})\boldsymbol{p}_{k(i)}$ and $R(\boldsymbol{\alpha})\boldsymbol{p}_{k(j)}$ with respect to $\boldsymbol{\alpha}$ evaluated at $\boldsymbol{\alpha} = 0$, as in Equation (24), then the uncertainty $u(d_{ij})$ associated with the distance d_{ij} due to rotation effects is given by

$$u^2(d_{ij}) = \sigma_{ER}^2 \Big(\boldsymbol{m}_i^\top \boldsymbol{m}_i + \boldsymbol{m}_j^\top \boldsymbol{m}_j - 2(\boldsymbol{m}_i^\top \boldsymbol{m}_j) e^{-d_{ij}^2/\lambda_{ER}^2}\Big),$$

where $\boldsymbol{m}_i = G_i \boldsymbol{n}_{ij}$, etc. If the same probe is used for both measurements, then $\boldsymbol{p}_i = \boldsymbol{p}_j = \boldsymbol{p}$, say, $\boldsymbol{m}_i = \boldsymbol{m}_j = \boldsymbol{m}$, say, and

$$u^2(d_{ij}) = 2\sigma_{ER}^2 \boldsymbol{m}^\top \boldsymbol{m} \Big(1 - e^{-d_{ij}^2/\lambda_{ER}^2}\Big).$$

For this latter case, the quantity $\boldsymbol{m}^\top \boldsymbol{m}$ depends on the relationship between $\boldsymbol{n}_{ij}$ and $\boldsymbol{p}$. If $\boldsymbol{p}$ is in the same direction as $\boldsymbol{n}_{ij}$ (unlikely to be so in practice) $\boldsymbol{m} = \boldsymbol{0}$. If $\boldsymbol{p}$ is orthogonal to $\boldsymbol{n}_{ij}$ (as is often the case), then $\boldsymbol{m}^\top \boldsymbol{m} = \boldsymbol{p}^\top \boldsymbol{p}$, then for the measurement of a distance using the same probe,

$$u(d_{ij}) \le \sqrt{2}\sigma_{ER} \|\boldsymbol{p}\| \Big(1 - e^{-d_{ij}^2/\lambda_{ER}^2}\Big)^{1/2}.$$

More generally,

$$u(d_{ij}) \leq \sqrt{2}\sigma_{ER}P\left(1 - e^{-d_{ij}^2/\lambda_{ER}^2}\right)^{1/2} \leq \sqrt{2}\sigma_{ER}P,$$

where P is the length of the longest probe involved.

6.6. Distance Measurement: Uncertainty Contribution from Spatially Correlated Probing Effects (P)

See Section 5.5. We assume the spatial correlation is isotropic and specified by variance σ_P^2 and length scale parameter λ_P. The spatial correlation parameter λ_P relates to chordal distance on the unit sphere and is usually chosen so that two points that are diametrically opposed on the unit sphere are associated with independent effects, i.e., λ_P is significantly smaller than 1. In general, a value of $\lambda_P = 1/2$ is appropriate. Suppose $\boldsymbol{x}_i$ is measured in probing direction $\boldsymbol{n}_i$ using probe offset $\boldsymbol{p}_{k(i)}$ with associated statistical parameters $\sigma_{P_0,k(i)}$, $\sigma_{P,k(i)}$ and $\lambda_{P,k(i)}$, etc., and $\boldsymbol{n}_{ij}$ is the unit vector pointing from $\boldsymbol{x}_i$ to $\boldsymbol{x}_j$. For the case of different probes, the model in Section 5.5 assumes that the probing effects are independent so that

$$u^2(d_{ij}) = \sigma_{P_0,k(i)}^2 + \sigma_{P_0,k(j)}^2 + \sigma_{P,k(i)}^2 + \sigma_{P,k(j)}^2.$$

For $\boldsymbol{p}_i = \boldsymbol{p}_j = \boldsymbol{p}$, etc.,

$$\begin{aligned} u^2(d_{ij}) = {} & \sigma_{P_0}^2(o_i^2 + o_j^2 - 2o_io_j) \\ & + \sigma_P^2\left(o_i^2 + o_j^2 - 2o_io_je^{-d_{P,ij}^2/\lambda_P^2}\right), \end{aligned}$$

where

$$o_i = \boldsymbol{n}_i^\top \boldsymbol{n}_{ij}, \quad o_j = \boldsymbol{n}_j^\top \boldsymbol{n}_{ij}, \quad d_{P,ij} = \|\boldsymbol{n}_j - \boldsymbol{n}_i\|.$$

It is usually the case that $\boldsymbol{n}_i$ and $\boldsymbol{n}_j$ are aligned with $\boldsymbol{n}_{ij}$. In this case, $o_i, o_j = \pm 1$, and we have

$$u^2(d_{ij}) = 4\sigma_{P_0}^2 + 2\sigma_P^2, \quad \boldsymbol{n}_i = -\boldsymbol{n}_j, \quad u^2(d_{ij}) = 0, \quad \boldsymbol{n}_i = \boldsymbol{n}_j. \tag{32}$$

The relationships above in Equation (32) show how the model accounts for the differences between uni-directional and bi-directional probing. For example, in measuring a step gauge, the probing effects do not contribute to the uncertainties associated with the distances between left-facing faces or between right-facing faces but contribute to the uncertainties in distances between left- and right-facing faces. In the comparison of two gauge blocks sitting side by side in which all four faces (two left-, two right-facing) are measured with the same probe, then the uncertainty contributions are such that

$$u^2(d_{12}) = u^2(d_{34}) = 4\sigma_{P_0}^2 + 2\sigma_P^2, \quad u^2(d_{12} - d_{34}) = 0.$$

6.7. Summary: Uncertainties Associated with Distances Due to the Influence Factors

In the sections above, we have considered the uncertainty contributions to distances due to a number of effects. In this section we summarise these results, giving typical uncertainty contributions in terms of a small number of statistical parameters.

Random effects (R). Statistical parameter σ_R.

$$u_R^2(d_{ij}) = 2\sigma_R^2.$$

Probe qualification effects (PQ). Statistical parameters σ_{PQ} representing the maximum probe qualification uncertainty. For distance measurements using the same probe, the contribution is zero. Otherwise,

$$u_{PQ}^2(d_{ij}) \leq 2\sigma_{PQ}^2.$$

Scale and squareness effects (S). Statistical parameters σ_S, $\sigma_{S,a}$ and σ_Q. For this model, the uncertainty in distance is approximated by

$$u_S^2(d_{ij}) \approx \left(\sigma_S^2 + \sigma_{S,a}^2 + \sigma_Q^2\right) d_{ij}^2.$$

If the measurements are aligned with an axis, the squareness component, represented by σ_Q, makes no contribution.

Spatially correlated location effects (ET). Statistical parameters σ_{ET} and λ_{ET}.

$$u_{ET}^2(d_{ij}) = 2\sigma_{ET}^2\left(1 - e^{-d_{ij}^2/\lambda_{ET}^2}\right) \leq 2\sigma_{ET}^2.$$

Spatially correlated rotation effects (ER). Statistical parameters σ_{ER}, λ_{ER} and the maximum probe length P.

$$u_{ER}^2(d_{ij}) \leq 2\sigma_{ER}^2 P^2\left(1 - e^{-d_{ij}^2/\lambda_{ER}^2}\right) \leq 2\sigma_{ER}^2 P^2.$$

Spatially correlated probing effects (P). Statistical parameters σ_{P_0}, σ_P, and λ_P:

$$u_P^2(d_{ij}) \leq 4\sigma_{P_0}^2 + 2\sigma_P^2.$$

Putting these formulæ together, we derive a summary estimate of the uncertainty $u(d)$ associated with length measurement given by

$$u^2(d) = \sigma_A^2 + \left(\sigma_S^2 + \sigma_{S,a}^2 + \sigma_Q^2\right) d^2 + 2\sigma_{ET}^2\left(1 - e^{-d^2/\lambda_{ET}^2}\right) + 2\sigma_{ER}^2 P^2\left(1 - e^{-d^2/\lambda_{ER}^2}\right), \quad (33)$$

with

$$\sigma_A^2 = 2\left(\sigma_R^2 + \sigma_{PQ}^2 + \sigma_P^2 + 2\sigma_{P_0}^2\right). \quad (34)$$

In Equation (33), it is seen that $u(d)$ is the sum of four components, the first independent of distance, the second directly proportional to distance, while the other two terms depend on the ratio of distance relative to a spatial correlation length.

6.8. Plausible Values for Statistical Parameters Based on an MPE Statement

The analysis above shows how the uncertainty $u(d)$ associated with length measurement depends on the various influence factors considered. The analysis provides an estimate of $u(d)$ in terms of the statistical hyper-parameters assigned to the influence factors. A statement of maximum permissible error can be used to derive plausible values on these statistical hyper-parameters or, at a minimum, provide upper bounds for them. Suppose the MPE statement is $|d - d^*| \leq A + d^*/B$. We can interpret this statement statistically as

$$Ku(d) \leq A + d/B,$$

where K is, say, 2 or 3. From the summary information given in Section 6.7 above and specifically Equation (33), for $d_{ij} \approx 0$, the uncertainty $u(d_{ij})$ is such that $u^2(d_{ij}) = \sigma_A^2$ which implies

$$\sigma_A^2 = 2\left(\sigma_R^2 + \sigma_{PQ}^2 + \sigma_P^2 + 2\sigma_{P_0}^2\right) \leq A^2/K^2 \quad (35)$$

in order to conform to the MPE statement. This inequality relates σ_A directly to A and puts constraints on the size of σ_A defined above and, therefore, on the statistical parameters σ_R, σ_{PQ}, σ_{P_0} and σ_P. Similarly, for larger distances, the MPE constraint implies

$$\sigma_S^2 + \sigma_{S,a}^2 + \sigma_Q^2 \leq \frac{u^2(d)}{d^2} \leq \frac{1}{d^2K^2}(A + d/B)^2 \approx \frac{1}{K^2B^2},$$

so that the scale and squareness hyper-parameters are effectively bounded by $1/(KB)$. The relationship

$$2\sigma_{ET}^2\left(1-e^{-d^2/\lambda_{ET}^2}\right)+2\sigma_{ER}^2P^2\left(1-e^{-d^2/\lambda_{ER}^2}\right)\leq u^2(d)\leq\frac{1}{K^2}(A+d/B)^2,$$

constrains the combined effect of the kinematic errors as specified by σ_{ET} and σ_{ER} along the the spatial correlation lengths λ_{ET} and λ_{ER}.

In general, given a summary estimate $u(d)$ of the uncertainty in distance due to the combined effects, we can evaluate

$$C(d)=\frac{Ku(d)}{A+d/B}. \tag{36}$$

If $C(d)\leq 1$ over the working volume, then the values of the statistical parameters do not violate the MPE statement. If $C_{\max}=\max_{d\leq L_{\max}}C(d)$ is the maximum value of $C(d)$ over the working volume, then the simple procedure of dividing all the statistical parameters representing standard deviations, σ_R, etc., by $C_{\max}$ will lead to conformance with the MPE statement.

The MPE statement can be used, along with any other information, expert judgement, etc., to guide the assignment of the statistical hyper-parameters. The assignment cannot be unique, as demonstrated in Section 3, but the MPE can be used to determine a range of plausible values for the parameters. Making an assignment involves setting a balance between the random effects, the scale and squareness effects and the translational and rotational effects.

Table 3 gives two examples of MPE statements, labelled MPE1 and MPE2, along with assignments of values for the statistical hyper-parameters that have been derived to be consistent with the MPE statements. MPE1 corresponds to a more accurate CMM relative to MPE2. Graphs of the MPE and uncertainty components associated with distance as a function of d derived for statistical parameters in Table 3 and expansion factor $K=2$ are shown in Figures 4 and 5. The figures shows that the statistical parameters conform to the MPE statements. The uncertainty contribution from scale and squareness effects is linear in d, while the spatially correlated location and rotation effects start off as linear in d but begin to level off for larger values of d. For both characterisations, the spatial correlation length scale parameter λ_{ER} associated with the rotation effects is larger than that λ_{ET} for the location effects and the levelling off occurs later for the rotation effects. For MPE2, associated with shorter spatial correlation lengths, the levelling off occurs earlier than that for MPE1.

Table 3. Two sets of statistical parameters estimated from MPE statements of the form $A+d/B$.

Effect	Parameter	Unit	MPE1	MPE2
MPE	A	µm	1.0	3.0
	B	mm	500	200
Repeatability	σ_R	µm	0.20	0.60
Scale, squareness	σ_S	10^{-6}	0.7	2.1
	$\sigma_{S,a}$	10^{-6}	0.7	2.1
	σ_Q	10^{-6}	0.7	2.1
Probe qualification	σ_{PQ}	µm	0.20	0.60
Location	σ_{ET}	µm	0.2	0.6
	λ_{ET}	mm	200	100.0
Rotation	σ_{ER}	µrad	4.0	12.0
	λ_{ER}	mm	400	200
	P	mm	50	50
Probing	σ_{P_0}	µm	0.10	0.30
	σ_P	µm	0.10	0.30
	λ_P	1	0.50	0.50

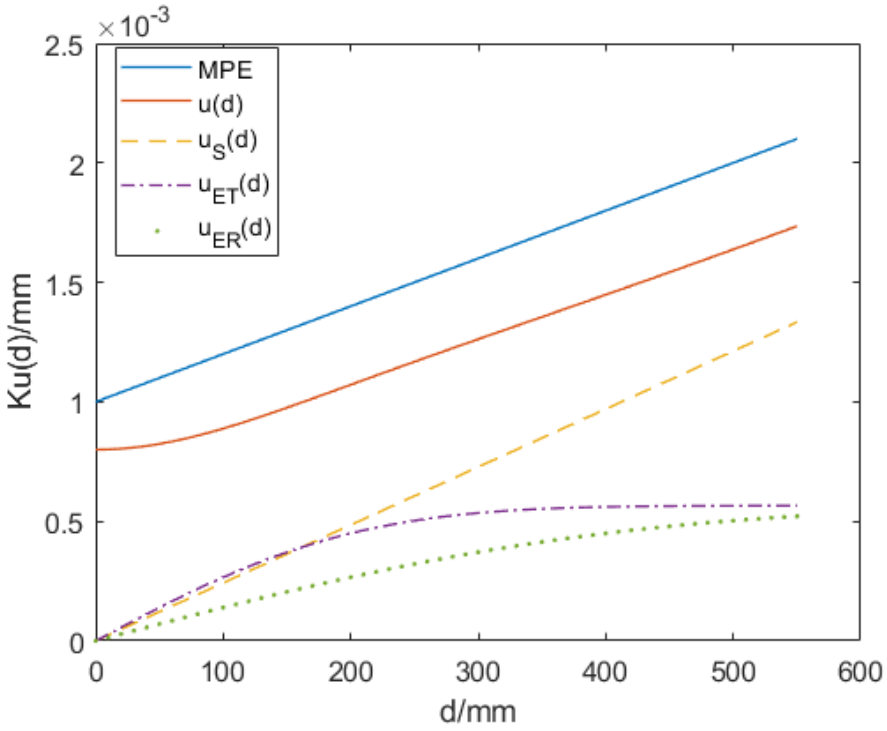

Figure 4. Graphs of the MPE and uncertainty of distance components as a function of d. The upper straight line is $A + d/B$, the solid line is $Ku(d)$ with $u(d)$ evaluated as in Equation (33). The other graphs give the uncertainty contributions $Ku_S(d)$ from scale and squareness effects, dotted straight line, $Ku_{ET}(d)$ from spatially correlated location effects, dashed line, and $Ku_{ER}(d)$ from spatially correlated rotation effects, dot–dashed line, derived from the statistical parameters in the column labelled MPE1 in Table 3 and expansion factor $K = 2$.

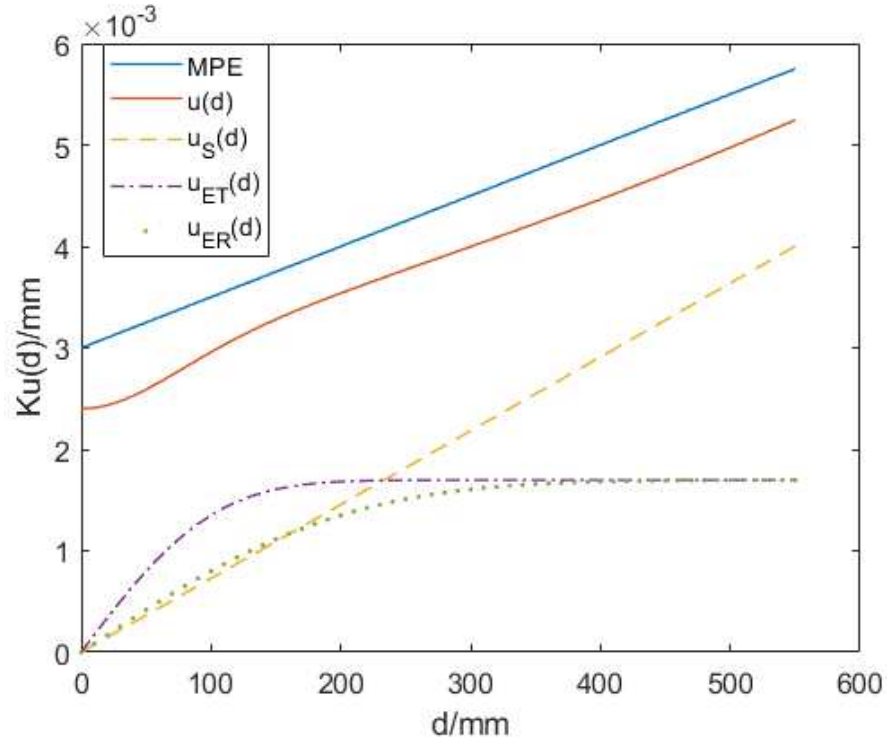

Figure 5. As in Figure 4 but derived from the statistical parameters in the column labelled MPE2 in Table 3.

7. Numerical Illustration: Measurement of a Step Gauge

The simulations involve characterisations of CMM behaviour based on the two MPE statements and statistical parameters given in Table 3. The calculations involve simulations of measurements of a step gauge with 26 steps each of nominal length 10 mm situated at 20 mm intervals along a measuring line. The simulations reported on here involve two scenarios. In each scenario, the step gauge is aligned with the x-axis so that measurements are not sensitive to squareness effects nor scale effects associated with the y- and z-axes.

Scenario I. This (realistic) scenario assumes (i) the 52 step faces are measured with the same probe with probe offset $\boldsymbol{p} = (0.0, 0.0, -20.0)^\top$ mm. In this scenario, the measured distances are not sensitive to probe qualification effects and the only rotation effect of importance is rotation about the y-axis, i.e., pitch along the x-axis.

Scenario II. This scenario (used for illustration) assumes (ii) the 26 left-facing faces are measured with a probe with offset $\boldsymbol{p}_L = (0.0, 20.0, 0.0)^\top$ mm and the 26 right-facing faces are measured with a probe with offset $\boldsymbol{p}_R = (0.0, -20.0, 0.0)^\top$ mm. In this scenario, the measured distances are sensitive to probe qualification effects. The measurements are also sensitive to rotation about the z-axis, i.e., yaw along both the x- and y-axes.

The associated features derived from the measurements are as follows:

d_{ij} The distances between all faces, with $d_{ij} = \|\boldsymbol{x}_i - \boldsymbol{x}_j\|$.
$d_{LL,ij}$ The distances between left-facing faces.
$d_{RR,ij}$ The distances between right-facing faces.
$d_{FF,k}$ The estimated length of each step.

The uncertainties associated with these distances have been calculated by evaluating the variance matrix V_X associated with the point cloud $\boldsymbol{x}_i$, $i = 1, \ldots, m = 52$, representing points on the centre of the 52 step gauge faces. The variance matrix V_X is constructed as in Equation (28), involving the various influence factors. The uncertainties associated with distances are calculated using Equation (29), decomposed as in Equation (30). These calculations do not depend on any of the simplifying assumptions used in Section 6 to derive compact formulæ for uncertainties associated with distances.

Figures 6 and 7 plot the estimated expanded uncertainty $Ku(d)$ with $K = 2$ associated with distances derived from measurements of a step gauge under scenario I and scenario II, respectively, and statistical parameters given in column 4 of Table 3, MPE1, for the different associated features discussed above. (The graphs corresponding to MPE2 show a similar behaviour.) The label 'LL' relates to distances between left-facing faces, 'RR' to distances between right-facing faces and 'FF' to the distances between the step faces for each step. Also plotted is the MPE function $A + d/B$ (upper straight line).

The two figures show that the uncertainties associated with left-facing faces and right-facing faces are the same for both scenarios since these distances are not sensitive to probe qualification effects and the rotation effects are essentially the same. We have assumed that the rotation errors are isotropic, i.e., the same for each axis so that a pitch about the x-axis, scenario I, has the same effect as yaw along the x-axis, scenario II, bearing in mind that each probe offset is of length 20 mm. In both cases, the uncertainties associated with distances involving both a left- and right-facing face are significantly larger because they are also are sensitive to probing effects. In the case of scenario II, these distances are also sensitive to yaw errors along the y-axes.

More insight into the uncertainty behaviour can be found by examining Tables 4 and 5, which give the standard uncertainties (column two) in micrometres associated with the distances between the first and second, first and 51st and first and 52nd (last) faces of the

step gauge for scenarios I and I and statistical parameters MPE1, and MPE2. We note the following from Table 4, scenario I, involving only one probe offset.

- The distance measurements are not sensitive to probe qualification effects.
- Measurements involving left-facing faces only are not sensitive to probing effects as they both involve the same probing direction.
- The uncertainties associated with scale effects are proportional to the distances, as would be expected.
- For the short distances, the spatially correlated translation and rotational effects make a very small uncertainty contribution.

We note the following from Table 5, scenario II, involving two probe offsets.

- Measurements involving left-facing faces only are not sensitive to probe qualification effects as they only involve one probe offset.
- Measurements involving left-facing faces only are not sensitive to probing effects as they both involve the same probing direction (as in scenario I).
- The rotational effects are significant for the measurement of the distance between the first and second face. The measurement of the first face involves one probe offset while the measurement of the second involves the second probe offset, which means that the CMM position differs by 40 mm as measured along the y-axis, so that yaw along the y-axis has an effect. Because the distance along the y-axis is small, 40 mm, relative to the spatial correlation length, these yaw errors are significantly correlated but because the two probe offsets are in different directions along the y-axis, these yaw errors do not cancel but instead have approximately double the effect. Only by including the relationship between rotational errors and probe offsets in the model, as described in Section 5.4, is it possible to capture this uncertainty behaviour.

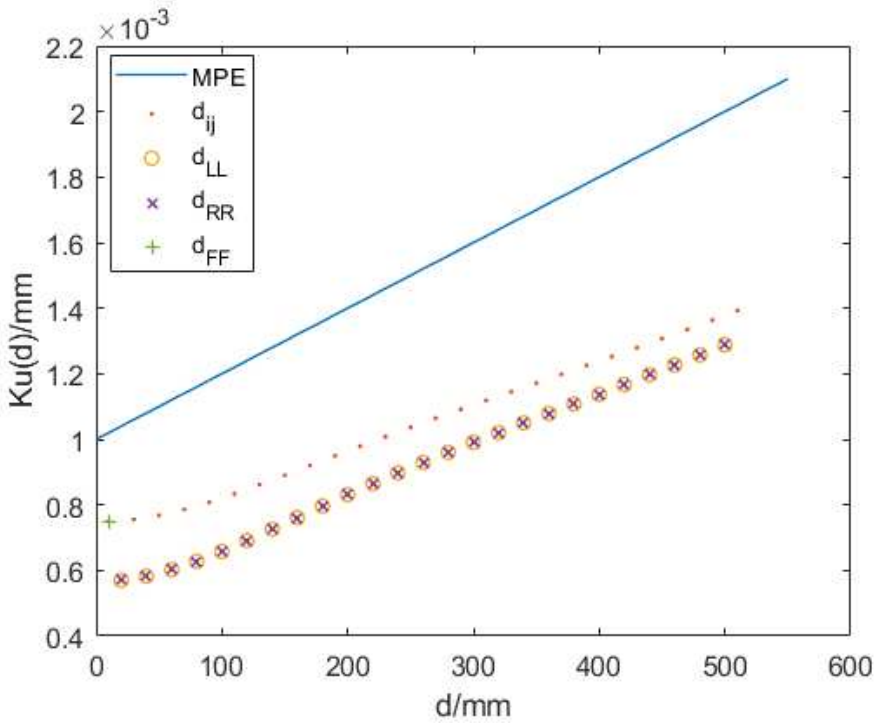

Figure 6. Estimated expanded uncertainty $Ku(d)$ with $K = 2$ associated with distances derived from measurements of a step gauge under scenario I and statistical parameters given by the third column of Table 3, MPE1. The label 'LL' relates to distances between left-facing faces, 'RR' to distances between right-facing faces and 'FF' to the distances between the step faces for each step. Additionally plotted is the MPE function $A + d/B$ (upper straight line).

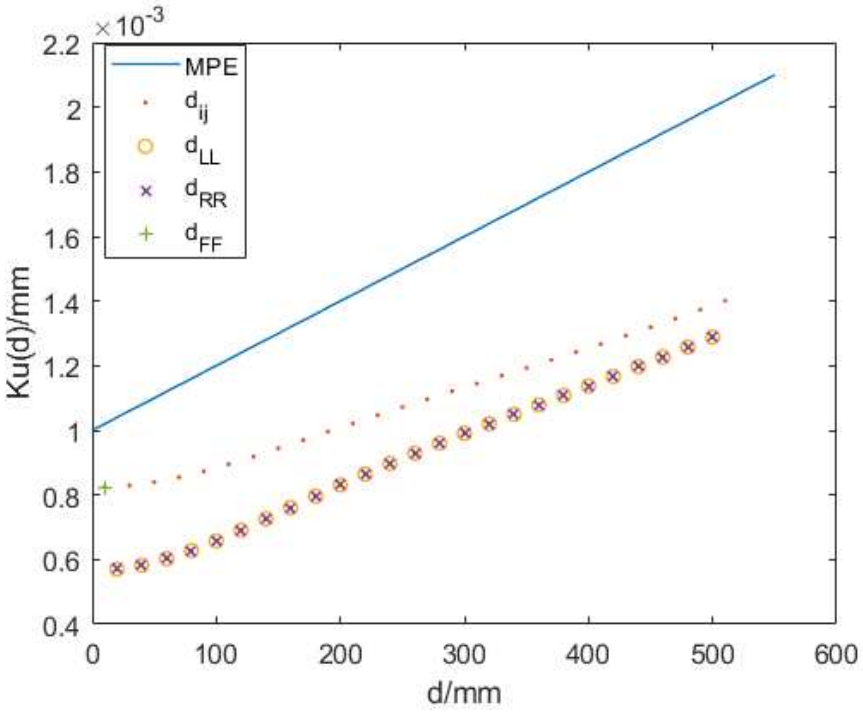

Figure 7. As Figure 6 but for statistical parameters given by the fourth column of Table 3, MPE2.

Table 4. Standard uncertainties (column three) in micrometres associated with the distances between the first and second, 51st and 52nd faces for the step gauge for scenario I and statistical parameters labelled MPE1, first four rows, and MPE2, second four rows, given in columns 4 and 5 of Table 3. Additionally shown (columns three and above) are the uncertainty contributions from the different influence factors, also in micrometres.

	d/mm	u	u_R	u_{PQ}	u_S	u_{ET}	u_{ER}	u_P
LR	10.00	0.37	0.28	0.00	0.01	0.01	0.00	0.24
LL	20.00	0.28	0.28	0.00	0.02	0.03	0.01	0.00
LL	500.00	0.64	0.28	0.00	0.49	0.28	0.10	0.00
LR	510.00	0.70	0.28	0.00	0.50	0.28	0.10	0.24
LR	10.00	1.13	0.85	0.00	0.03	0.08	0.02	0.73
LL	20.00	0.87	0.85	0.00	0.06	0.17	0.03	0.00
LL	500.00	1.94	0.85	0.00	1.48	0.85	0.34	0.00
LR	510.00	2.10	0.85	0.00	1.51	0.85	0.34	0.73

Table 5. As Table 4 but for scenario II.

	d/mm	u	u_R	u_{PQ}	u_S	u_{ET}	u_{ER}	u_P
LR	10.00	0.41	0.28	0.14	0.03	0.06	**0.16**	0.20
LL	20.00	0.28	0.28	0.00	0.02	0.03	0.01	0.00
LL	500.00	0.64	0.28	0.00	0.49	0.28	0.10	0.00
LR	510.00	0.70	0.28	0.14	0.51	0.28	0.12	0.20
LR	10.00	1.27	0.85	0.42	0.09	0.34	**0.47**	0.60
LL	20.00	0.87	0.85	0.00	0.06	0.17	0.03	0.00
LL	500.00	1.94	0.85	0.00	1.48	0.85	0.34	0.00
LR	510.00	2.10	0.85	0.42	1.52	0.85	0.34	0.60

8. Concluding Remarks

This paper has been concerned with the evaluation of uncertainties associated with point clouds and distances as measured by a CMM. The uncertainty evaluation methodology is model-based, following the principles of the GUM and the law of propagation of uncertainty and has considered a range of influence factors—repeatability effects, probe qualification effects, scale and squareness effects, kinematic/geometrical errors, and probing effects. Using plausible models of CMM behaviour for each of these effects, it has been possible to derive the sensitivities of point clouds and derived distances to the influence factors and express their contribution to length measurement uncertainty in terms of straightforward formulæ depending on a small number of statistical hyper-parameters. The methodology has been illustrated on measurements of a step gauge. The evaluation of the uncertainties requires no Monte Carlo simulations and can be (and has been) implemented in spreadsheets, for example.

The fact that the uncertainty in length measurement for each of the effects can be evaluated explicitly means that their contribution to the CMM's maximum permissible error (MPE) can be also be evaluated. Conversely, a valid statement of MPE can be used to constrain the values of the statistical hyper-parameters and derive point cloud uncertainties that are consistent with the MPE statement.

Funding: This work is based on research undertaken as part of the European Metrology Programme for Innovation and Research (EMPIR), through project 17NRM03: *Evaluating Uncertainty in Coordinate Measurement*—EUCoM. The EMPIR initiative was co-funded by the European Unions Horizon 2020 research and innovation programme and the EMPIR Participating States.

Institutional Review Board Statement: Not applicable.

Informed Consent Statement: Not applicable.

Data Availability Statement: The original contributions presented in the study are included in the article, further inquiries can be directed to the corresponding author.

Acknowledgments: The author is grateful to EUCoM project partners for input into this work, in particular to Alessandro Balsamo, INRIM, Italy, the EUCoM project coordinator, for his many insights and support. The author is also grateful to the anonymous referees for their helpful comments and corrections.

Conflicts of Interest: The author declares no conflict of interest.

References

1. Hocken, R.J.; Pereira, P.H. *Coordinate Measuring Machines and Systems*; CRC Press: Boca Raton, FL, USA, 2012.
2. BIPM. *The International System of Units (SI Brochure (EN))*, 9th ed.; NIST Special Publication: Gaithersburg, MD, USA, 2019.
3. *JCGM 100:2008*; Evaluation of Measurement Data—Guide to the Expression of Uncertainty in Measurement. Joint Committee for Guides in Metrology: Sèvres, France, 2008.
4. Sładek, J.A. *Coordinate Metrology—Accuracy of Systems and Measurement*; Springer: Berlin/Heidelberg, Germany, 2016.
5. Automotive Industry Action Group. *Measurement Systems Analysis: Reference Manual*, 4th ed.; Automotive Industry Action Group: Southfield, MI, USA, 2010.
6. *ISO 5725-1*; Accuracy (Trueness and Precision) of Measurement Methods and Results—Part 1: General Principles and Definitions. International Organization for Standardization: Geneva, Switzerland, 1994.
7. *ISO 5725-2*; Accuracy (Trueness and Precision) of Measurement Methods and Results—Part 2: Basic Method for the Determination of Repeatability and Reproducibility of a Standard Measurement Method. International Organization for Standardization: Geneva, Switzerland, 2019.
8. Montgomery, D.C. *Design and Analysis of Experiments*, 8th ed.; John Wiley & Sons: New York, NY, USA, 2013.
9. *JCGM 101:2008*; Evaluation of Measurement Data —Supplement 1 to the "Guide to the Expression of Uncertainty in Measurement"—Propagation of Distributions Using a Monte Carlo Method. Joint Committee for Guides in Metrology: Sèvres, France, 2008.

10. *JCGM 102:2011*; Evaluation of Measurement Data—Supplement 2 to the "Guide to the Expression of Uncertainty in Measurement"—Extension to any Number of Output Quantities. Joint Committee for Guides in Metrology: Sèvres, France, 2011.
11. *Evaluation of Uncertainty Associated with Coordinate Measurement*; EURAMET: Braunschweig, Germany. Available online: https://eucom-empir.eu/ (accessed on 1 December 2024).
12. Sato, O.; Takatsuji, T.; Miura, Y.; Nakanishi, S. GD&T task specific measurement uncertainty evaluation for manufacturing floor. *Meas. Sens.* **2021**, *18*, 100141. [CrossRef]
13. Sato, O.; Takatsuji, T.; Balsamo, A. Practical experiment design of task-specific uncertainty evaluation for coordinate metrology. In *Advanced Mathematical and Computational Tools for Metrology XII*; Pavese, F., Forbes, A.B., Yang, N.F., Chunovkina, A., Eds.; World Scientific: Singapore, 2022; pp. 381–389.
14. Gąska, A.; Harmatys, W.; Gąska, P.; Gruza, M.; Gromczak, K.; Ostrowska, K. Virtual CMM-based model for uncertainty estimation of coordinate measurements performed in industrial conditions. *Measurement* **2017**, *98*, 361–371. [CrossRef]
15. Heißelmann, D.; Franke, M.; Rost, K.; Wendt, K.; Kistner, T.; Schwehn, C. Determination of measurement uncertainty by Monte Carlo simulation. In *Advanced Mathematical and Computational Tools in Metrology and Testing XI*; Forbes, A.B., Zhang, N.F., Chunovkina, A., Eichstädt, S., Pavese, F., Eds.; World Scientific: Singapore, 2019; pp. 192–202. [CrossRef]
16. Manlay, J.F.; Charki, A.; Delamarre, A. A virtual CMM to estimate uncertainties. *Int. J. Metrol. Qual. Eng.* **2024**, *15*, 21. [CrossRef]
17. Phillips, S.; Borchardt, B.; Sawyer, D.; Estler, W.; Ward, D.; Eberhardt, K.; Levenson, M.; McClain, M.; Melvin, B.; Hopp, T.; et al. The Calculation of CMM measurement uncertainty via The Method of Simulation by Constraints. *Proc. ASPE* **1997**, 443–446.
18. Sładek, J.; Gąska, A. Evaluation of coordinate measurement uncertainty with use of virtual machine model based on Monte Carlo method. *Measurement* **2012**, *45*, 1564–1575. [CrossRef]
19. Trapet, E.; Waldele, F. The virtual CMM concept. In *Advanced Mathematical Tools in Metrology, II*; Ciarlini, P., Cox, M.G., Pavese, F., Richter, D., Eds.; World Scientific: Singapore, 1996; pp. 238–247.
20. Balsamo, A.; Franke, M.; Trapet, E.; Wäldele, F.; De Jonge, L.; Vanherck, P. Results of the CIRP-EUROMET intercomparison of ball plated-based techniques for determining CMM parametric errors. *Ann. CIRP* **1997**, *46*, 463–466. [CrossRef]
21. Kunzmann, H.; Trapet, E.; Waldele, F. A uniform concept for calibration, acceptance test and periodic inspection of co-ordinate measuring machines using reference objects. *Ann. CIRP* **1990**, *39*, 561–564. [CrossRef]
22. Cox, M.G.; Forbes, A.B.; Harris, P.M.; Peggs, G.N. Determining CMM behaviour from measurements of standard artefacts. In *Technical Report CISE 15/98*; National Physical Laboratory: London, UK, 1998.
23. Forbes, A.B. Approximate models of CMM behaviour and point cloud uncertainties. *Meas. Sens.* **2021**, *18*, 100304. [CrossRef]
24. Cox, M.G.; Harris, P.M. SS*f*M Best Practice Guide No. 6, Uncertainty evaluation. In *Technical Report MS 6*; National Physical Laboratory: London, UK, 2010.
25. Golub, G.; Van Loan, C. *Matrix Computations*, 4th ed.; Johns Hopkins University Press: Baltimore, MA, USA, 2013.
26. Linares, J.M.; Goch, G.; Forbes, A.; Sprauel, J.M.; Clément, A.; Härtig, F.; Gao, W. Modelling and traceability for computationally-intensive precision engineering and metrology. *CIRP Ann. Manuf. Technol.* **2018**, *67*, 815–838. [CrossRef]
27. Forbes, A.B. Sensitivity analysis for Gaussian associated features. *Appl. Sci.* **2022**, *12*, 2808. [CrossRef]
28. *ISO 10360*; Co-Ordinate Metrology: Performance Assessment of Co-Ordinate Measuring Machines. International Organization for Standardization: Geneva, Switzerland, 1995.
29. Wojtyła, M.; Rosner, P.; Płowucha, W.; Forbes, A.B.; Savio, E.; Balsamo, A. Determination of uncertainty of coordinate measurements on the basis of the formula for EL, MPE. *Measurement* **2023**, *222*, 113635. [CrossRef]
30. Balsamo, A. Effects of Arbitrary Coefficients of CMM Error Maps on Probe Qualification. *CIRP Ann. Manuf. Technol.* **1995**, *44*, 475–478. [CrossRef]
31. Cressie, N.; Wikle, C.K. *Statistics for Spatio-Temporal Data*; Wiley: Hoboken, NJ, USA, 2011.
32. Rasmussen, C.E.; Williams, C.K.I. *Gaussian Processes for Machine Learning*; MIT Press: Cambridge, MA, USA, 2006.
33. Zhang, G.; Ouyang, R.; Lu, B.; Hocken, R.; Veale, R.; Donmez, A. A displacement method for machine geometry calibration. *Ann. CIRP* **1988**, *37*, 515–518. [CrossRef]
34. Cresto, P.C. Self-calibration with application to CMMs geometry error correction. In *International Workshop on Advanced Mathematical Tools for Metrology, Turin*; Ciarlini, P., Cox, M.G., Monaco, R., Pavese, F., Eds.; World Scientific: Singapore, 1994; pp. 167–174.
35. Kruth, J.P.; Vanherk, P.; de Jonge, L. Self-calibration method and software error correction for three dimensional co-ordinate measuring machines using artefact measurements. *Measurement* **1994**, *14*, 1–11. [CrossRef]
36. Kennedy, M.C.; O'Hagan, A. Bayesian calibration of computer models. *J. R. Sat. Soc. B* **2001**, *64*, 425–464. [CrossRef]
37. Abrahamsen, P. *A Review of Gaussian Random Fields and Correlation Functions*; Norsk Regnesentral/Norwegian Computing Centre: Oslo, Norway, 1997.